

Study of High-Energy Photoproduction with Positron-Annihilation Radiation. I. Three-Prong Events*

Y. Eisenberg, B. Haber, E. E. Ronat, A. Shapira, Y. Stahl, and G. Yekutieli
Weizmann Institute of Science, Rehovoth, Israel

and

J. Ballam, G. B. Chadwick, M. M. Menke, and P. Seyboth†
Stanford Linear Accelerator Center, Stanford University, Stanford, California 94305

and

S. Dagan and A. Levy
Tel-Aviv University, Tel-Aviv, Israel
(Received 21 July 1971)

The photoproduction of resonances has been studied in three exposures of a hydrogen bubble chamber to positron-annihilation radiation of 4.3-, 5.25-, and 7.5-GeV nominal energies. The general analysis procedure and results on the three-prong-event topology are presented. We study the highly constrained reaction $\gamma p \rightarrow p\pi^+\pi^-$ over the energy range 2–8 GeV and the reactions $\gamma p \rightarrow p\pi^+\pi^-\pi^0$ and $\gamma p \rightarrow n\pi^+\pi^-\pi^0$ at the annihilation energies. Cross sections are given. Using various models to parametrize the ρ^0 “elastic” reaction we find the mean t slope to be $7.1 \pm 0.4 \text{ GeV}^{-2}$ and its forward cross section to decrease from $130 \mu\text{b GeV}^{-2}$ at 3.3 GeV to $\sim 100 \mu\text{b GeV}^{-2}$ at 7.5 GeV. The cross section for $\gamma p \rightarrow \omega p$ is decomposed into one-pion exchange (OPE) and a diffractive part, $\sigma_D(\omega)$, which is found to be $1.5 \pm 0.3 \mu\text{b}$. $\sigma(\rho^0)/\sigma_D(\omega)$ is then 9.5 ± 2.3 . In comparing vector-meson production with Compton scattering via vector-meson dominance, we find that for $\gamma_p^2/4\pi = 0.32 \pm 0.03$ there is good agreement at all s and t where comparison may be made ($E_\gamma = 5\text{--}8 \text{ GeV}$). In a search for $\rho' \rightarrow 2\pi$, we find, at the 90% confidence level, $\sigma_{\rho'}(1250) < 0.3 \mu\text{b}$ and $\sigma_{\rho'}(1650) < 0.1 \mu\text{b}$ per 100-MeV width. Inelastic peripheral ρ^0 production is seen, but with present statistics we cannot identify specific nucleon isobars associated with it. Quasi-two-body reactions $\gamma p \rightarrow \pi^-\Delta^{++}$, $\rho^-\Delta^{++}$, and $A_1^+ n$ are observed, decreasing with photon energy like E_γ^{-a} . For the first two we find $a = 1.74 \pm 0.16$ and 0.6 ± 0.2 , respectively. We conclude that if the reaction $\gamma p \rightarrow \rho^-\Delta^{++}$ is due to an OPE process, the required $\rho \rightarrow \pi\gamma$ width ($\sim 0.5 \text{ MeV}$) is much in excess of the value predicted by SU(3).

I. INTRODUCTION

We describe here a hydrogen-bubble-chamber experiment to study high-energy photoproduction of resonances up to an incident energy of 8.2 GeV, using a collimated beam of electron-positron-annihilation radiation to provide photons of energy known to $\pm 2\%$. Knowledge of the incident photon energy allows constrained fits to be made to the charged-particle measurements of reactions with a neutral and hence unmeasured particle in the final state. Previous bubble-chamber studies^{1,2} as well as streamer-chamber work³ have used electron bremsstrahlung beams and hence the event measurements had one less constraint. With a clean separation of such reactions from multineutral production we may therefore obtain a more complete picture of resonance photoproduction in the high-energy region. Some preliminary results are already published.^{4,5} In this report we give full results on three-prong events, with particular

emphasis on the vector mesons; five-prong results will be given later. We also note that preliminary data from a bubble-chamber study using polarized photons has been reported.⁶⁻⁸

The bubble-chamber exposures were made at three mean annihilation photon energies of 4.3, 5.25, and 7.5 GeV. The 4.3-GeV film was measured and analyzed by the Weizmann Institute Group, the 5.25-GeV film by the SLAC Group, and the 7.5-GeV film by all groups. Since close collaboration during the exposures and analysis was maintained, we present here all the data obtained as essentially from a single experiment so as to enhance the statistical accuracy and to be able to discuss the energy dependence of resonance photoproduction. In addition to those events with zero or one missing neutral particle produced by the annihilation-radiation quasi-monochromatic peak, we also obtained a large number of events with no missing neutral particle from the positron-electron and positron-proton bremsstrahlung, and data

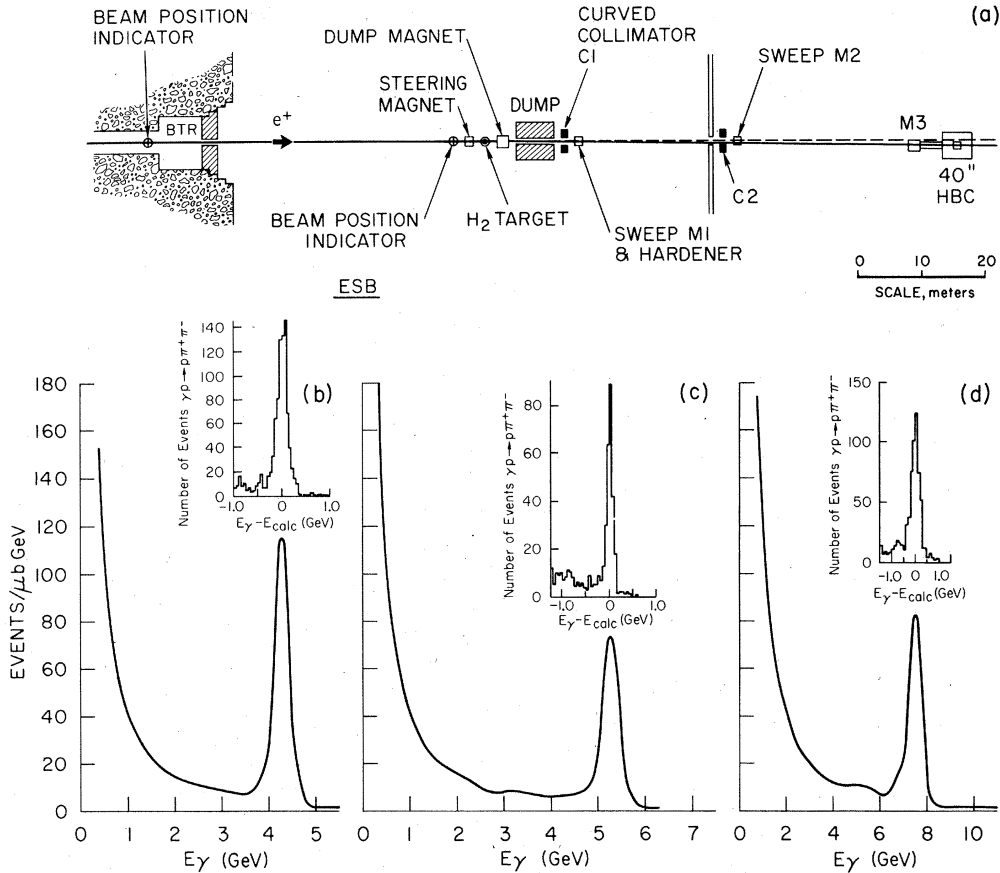


FIG. 1. (a) Layout of the positron-annihilation beam; (b) photon spectrum in the bubble chamber as deduced from measurements of the reaction $\gamma p \rightarrow p\pi^+\pi^-$ and normalized to microbarn equivalents from e^+e^- pair-production measurements. Positron energy 8.5 GeV, mean production angle 11.8 mrad. The inset shows the distribution of energies E_γ found for 3C (3-constraint) fits about that calculated from the event vertex position in the chamber, illustrating the narrowing effect; (c) same for 5.25-GeV run; $E_+ = 10$ GeV, $\bar{\theta} = 9.4$ mrad; (d) same for 7.5-GeV run; $E_+ = 12$ GeV, $\bar{\theta} = 7.15$ mrad.

from these reactions are also presented. In this work we do not present an analysis of strange-particle-producing events.

The photon beam and its characteristics are described in Sec. II, scanning and measuring details are given in Sec. III, and a discussion of the determination of reaction cross sections is presented in Sec. IV. The experimental data on the three-body final state is given in Sec. V, with greatest emphasis on the ρ^0 meson production and distinguishing between model-dependent and model-independent data. Section VI gives experimental data on the four-body final states. Section VII compares vector-meson production with the vector-dominance model.

II. BEAM AND BUBBLE CHAMBER

The positron-annihilation photon beam at SLAC has been described in detail elsewhere.⁹ Here we shall briefly outline the beam principles in order

to give an understanding of the beam spectrum and the energy resolution. Figure 1(a) shows a schematic representation of the beam setup. A positron beam of up to $E = 12$ GeV, resolved to $\pm 0.5\%$, is produced by a radiator placed at the one-third point in the 2-mile SLAC accelerator, and is focused to a spot of about 3-mm diameter with beam divergence $< 10^{-5}$ rad at a 15-cm liquid-hydrogen cell. Here the positrons annihilate with electrons in the hydrogen atoms. The incident direction of the positrons is monitored to ± 0.1 mrad by two beam position indicators, while the outgoing photons are collimated into a beam at 7–11 mrad to the positron direction by two collimators, so that a vertical sheet of photons traverses the SLAC 40-in. hydrogen bubble chamber. Three sweeping magnets clean up the beam, one of which contains ~ 1 radiation length of lithium hydride for beam hardening. The positron intensity was set to give about 14 e^+e^- pairs per burst in the chamber, and the flashes

TABLE I. Parameters and statistics of the three exposures.

Central photon energy (GeV)	4.3	5.25	7.5
Resolution (%)	± 2.0	± 2.0	± 2.0
Positron energy (GeV)	8.5	10.0	12.0
Central production angle (mrad)	11.9	9.4	7.15
Photons/frame, $k > 0.9k_A$	~ 54	~ 70	~ 30
Total pairs/frame in scanning volume	15.8	16.2	11.7
Total frames	300 000	252 000	940 000
Total event measured	10178	9153	$\sim 24\ 000$

were suppressed if the intensity fluctuated beyond limits. The bubble chamber is a 40-in. diameter cylinder, 20 in. deep, with Scotch-Lite illumination. The central field is 26 kg, uniform over the illuminated volume to $\pm 4\%$.

The resulting photon spectrum may be seen in Figs. 1(b)–1(d). It is expressed for each of the three energy settings as the number of events expected to be found in our fiducial volume for a reaction with 1- μ b cross section per GeV of incident photon energy interval. The prominent high-energy peaks are from the annihilation reactions

$$e^+ + e^- \rightarrow 2\gamma, \quad (1)$$

producing photons with a unique energy-angle relation. At angle θ the photon energy K_A is given by¹⁰

$$K_A = E(1 + E\theta^2/2M_e)^{-1}, \quad (2)$$

where M_e is the mass of the electron. The effective energy resolution obtained through collimation is ultimately limited by the radiative tail (emission of extra-low-energy photons) so that the sharp spike expected at energy K_A is actually transformed to a cusplike spectrum $\sim (K_A - K)^{-1}$. The photon energy resolution is further limited by the finite beam spot size and angular definition of the beam and collimators. In this experiment the production angle θ (between 7 and 12 mrad) was defined by the position of the event vertex in the bubble chamber

rather than by a very tight collimation. We therefore obtained a spectrum of annihilation photons with a fairly large spread of photon energies, but for individual event positions in the chamber the energy was known *a priori* to an accuracy of $\pm 2\%$. The inset spectra of Figs. 1(b)–1(d) shows the difference between this value (E_{calc}) and the energy obtained by measuring the highly constrained [three-constraint (3C)] reaction $\gamma p \rightarrow p\pi^+\pi^-$, illustrating the narrowing effect.

In addition to the annihilation photons, the beam contains a background due to bremsstrahlung from e^+ on electrons and nuclei, which was not overwhelming because the intensity falls much more rapidly with θ than does the annihilation intensity. The e^+e^- bremsstrahlung has a maximum energy at any θ given by Eq. (2). As will be described, multineutral production events from photons with energy $< K_A$ will not be confused with single neutral events. For photons of energy $> K_A$, confusion can result, but the e^+ -nucleus bremsstrahlung component is made small by the use of a hydrogen radiator, as well as being suppressed at large angles by the proton form factor.

The three exposures were made by setting the positron energy and photon production angle as close to those for symmetric photon production as possible.⁹ For the high-energy run, the maximum available positron energy was 12 GeV and a slightly

TABLE II. Reaction hypotheses tested for three-prong events.

Reaction	Source	Notation	Number of fits at:		
			4.3 GeV	5.25 GeV	7.5 GeV
(1) $\gamma p \rightarrow p\pi^+\pi^-$	Annih	$p+-A$	823	519	810
	Brems	$p+-B$	3917	4020	11 868
(2) $\gamma p \rightarrow p\pi^+\pi^-\pi^0$	Annih	$p+-0A$	832	943	1689
	Brems	$p+-0B$	1571	2058	5608
(3) $\gamma p \rightarrow n\pi^+\pi^+\pi^-$	Annih	$n++-A$	479	339	592
	Brems	$n++-B$	1313	1384	3809
(4) $\gamma p \rightarrow p\pi^+\pi^-MM$	Annih	$p+-MM$	2403	3001	7397
(5) $\gamma p \rightarrow \pi^+\pi^+\pi^-MM$	Annih	$++-MM$	1792	1723	4401

asymmetric setting was necessary. Table I shows the beam conditions and number of pictures obtained at each nominal energy.

III. SCANNING, MEASURING, AND HYPOTHESIS FITTING

The bubble-chamber photographs contain about 200 times more e^+e^- pairs than hadronic events, so that the pictures were generally crowded with pair tracks. We therefore made two independent scans for events in the first $\frac{2}{3}$ of the chamber, resolving identification differences in a third pass. Pairs were counted in the same fiducial volume every 100 frames for the flux determination, and in approximately half of these frames all pairs were measured. Between 90% and 94% of all events had successful measurements after three passes, the majority of those failing having short scattered tracks or vertex confused by low-energy pair spirals. In a 10% sample of the film it was checked that pairs failing reconstruction had no energy bias. The event geometries were obtained and fitted to the hypotheses shown in Table II, according to topology using the TVGP-SQUAW kinematics programs. This table also defines the mnemonic notation we shall use to identify these reactions in the remainder of the paper. Events fitting the reactions $\gamma p \rightarrow pK^+K^-$ and $\gamma p \rightarrow pK^+K^-\pi^+\pi^-$ better than the topologically equivalent π final states were eliminated from the sample, as were events with track ionization or decays distinguishable as K mesons. No good separation of nondecaying fast K 's in reactions with a neutral was possible, and this background was neglected. Proton-pion ambiguities were resolved where possible on the basis of visual ionization checks by physicists.

Since the alignment of the chamber with respect to the beam is subject to uncertainty, the target position in the bubble-chamber coordinates was determined by projecting back the measured pair track directions. The positron direction at the target was obtained in the same coordinates by requiring the reconstructed pair energies to have as narrow a peak as possible around the value given by Eq. (2), with E determined by the beam switchyard magnet settings. Each hypothesis was tried first assuming production by an annihilation photon with energy and direction determined by the measured vertex position in the chamber. Reaction (1), p^+-A , gives a 4-constraint fit, reactions (2), p^+-0A , and (3), $n^{++}-A$, a 1-constraint fit, while reactions (4), p^+-MM , and (5), $+-MM$, give no constraints. Then reactions (1), (2), and (3) were tried again without the energy constraint. Each well-measured event, therefore, has at least one missing-mass (MM) value from hypothesis (4) or

(5). For events either with a proton of momentum <1.3 GeV/c, or with all positive tracks ≤ 1.3 GeV/c, the missing mass is unique because all but one missing-mass hypothesis was excluded by the ionization check.

At this point it is useful to review some features of photoproduction kinematics. In the laboratory system, let k_T be the *true* energy of the photon producing an event, k the value *assumed* in the missing-mass fit. Let E_0 , p_0 , m_0 , and θ_0 be the energy, momentum, mass, and production angle with respect to the beam of the *actual neutral system* of particles. In the bubble chamber the momentum of an ionization-ambiguous track is measured correctly. Let $\alpha = (\text{assumed track energy minus true track energy}) \approx (m_f^2 - m_T^2)/2p$, where m_f is the mass assigned to an ambiguous track of momentum p ($p > 1.3$ GeV/c) while m_T is the true mass. We may then show that the calculated neutral mass m_c is given by

$$m_c^2 = m_0^2 + 2(k - k_T)(E_0 - p_0 \cos \theta_0) - 2\alpha(E_0 - k + k_T - \frac{1}{2}\alpha). \quad (3)$$

If the ionization-ambiguous track is assigned its correct mass, $\alpha = 0$, and we see that for true photon energy k_T less than the expected annihilation energy, m_c is always *greater* than the true missing mass, although a fast forward neutral system will make the missing mass insensitive to the assumed photon energy: In particular, events of the type p^+- will almost always fit p^+-0 . The only multineutral events which will be assigned an annihilation single neutral hypothesis are from the e^+p bremsstrahlung photons with energy $> K_A$, and as may be seen from the spectra of Fig. 1, will make negligible contamination. For the ionization-ambiguous events wrongly assigned, it turns out that those with a neutron in the final state ($\alpha > 0$) generally have low enough E_0 and high enough m_0 to make the overlap with the $p^+\pi^-\pi^0$ hypothesis small. Those with a fast proton, however, represent a considerable overlap and must be treated more carefully.

In Fig. 2(a) we show the missing mass calculated for *all* events failing a fit to p^+-A or p^+-B ($\chi^2 > 25$), with ionization consistent with p^+-MM . In Fig. 2(b) we show the same quantity for events consistent with $+-MM$. The peaks corresponding to single- π^0 and single-neutron production are evident. In Fig. 2(a) the superimposed curve A represents the expected missing-mass distribution for multi- π^0 events, as obtained from five-prong events by ignoring two of the measured π tracks. The long tail at low masses represents the expected contributions from events with $E_\gamma > K_A$. Curve B shows the shape expected for annihilation

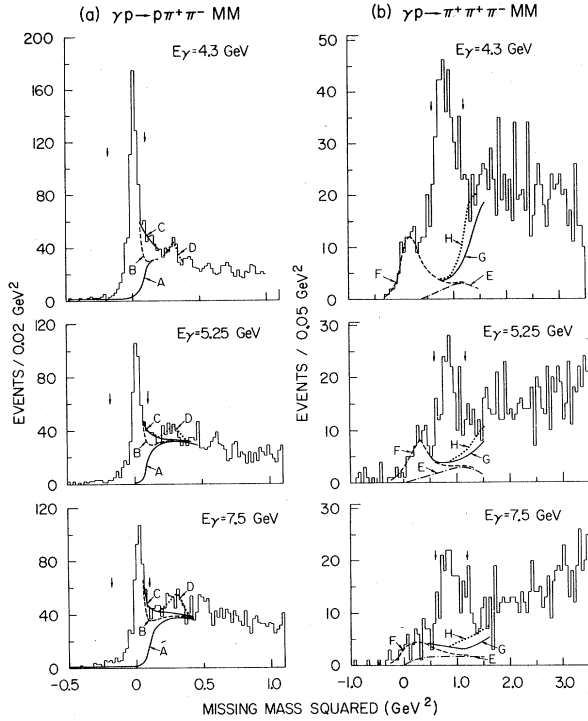


FIG. 2. (a) Missing mass squared, as defined in text, for all events consistent by ionization with the reaction $\gamma p \rightarrow p\pi^+\pi^-$ plus neutrals at the three photon energy settings; (b) same for events consistent by ionization with $\gamma p \rightarrow \pi^+\pi^+\pi^-$ plus neutrals. Events with fast protons appear in both (a) and (b).

events alone while curve C includes the $p+-0B$ events. Curve D shows η^0 production expected from the number of $\eta^0 \rightarrow \pi^+\pi^-\pi^0$ decays observed in the five-prong topology. We define a candidate for $p+-0A$ as having a 1C fit to that hypothesis with confidence level >0.005 and $-0.18 < MM^2 < 0.10$ GeV^2 . The purity of this sample is estimated to be $\geq 90\%$.

In the case of $n++-A$ the contamination is larger. In Fig. 2(b) the superimposed curves show how the background is made up of (a) $p+-0$ (A or B) with fast protons ambiguous with π^+ (curve F), (b) multi- π^0 production with a fast proton (curve E), (c) neutron-multi-neutrals as obtained from five prongs by ignoring the proton and one pion (curve G). Curve H shows the expected $n++-$ events from bremsstrahlung. Source (b) is the most difficult to estimate as such events produce a continuous band in MM^2 across the neutron-mass-peak region, and we may only assign "reasonable" limits to this contamination (10–20%) which are reflected in the cross-section uncertainties. We define a candidate for $n++-A$ as an event with a 1C fit of confidence level >0.005 and $0.6 < MM^2 < 1.2$ GeV^2 . The purity

of the sample selected varies from $\sim 85\%$ at 4.3 GeV to $\sim 75\%$ at 5.25 and 7.5 GeV.

In addition to the backgrounds discussed above, there was further uncertainty introduced from events of the correct reaction but produced by bremsstrahlung photons close enough in energy to the annihilation peak so that measurement errors allowed a 1C fit. Such uncertainties were handled by a Monte Carlo simulation as described in Sec. IV.

IV. CROSS-SECTION DETERMINATIONS

In a bubble-chamber study of photoproduction, the cross section σ may be obtained in a straightforward and precise manner: If e^+e^- pairs and events are found in the identical fiducial volume, we have

$$\sigma(\text{events}) = \frac{\text{number of events}}{\text{number of pairs}} \sigma(\text{pair}), \quad (4)$$

where $\sigma(\text{pair})$ is known to an accuracy $\sim 0.5\%$.¹¹ The corrections which must be applied are for the following effects:

- (1) scanning and measuring losses (a) of random nature, which are estimated by the double scan, and (b) systematic losses of three-prong events with short protons which can be confused with pairs,
- (2) distortion of the e^+e^- -pair energy spectrum because of multiple scattering and undetected energy loss through bremsstrahlung radiation along the lepton track,
- (3) loss of events from the individual reactions because of poor measurement, which are excluded by the fitting process and the cuts described in Sec. III,
- (4) events accepted, but actually from other reactions.

In addition to the above corrections and associated uncertainty, in the determination of single-resonance-production cross sections, some of the signal seen may in fact be formed in the contaminating reactions and will make the cross section appear larger. Such effects are important only for resonances decaying into only visible particles, as has been discussed in the ABBHBM publications.²

The correction (1) (b) was estimated from the copious $p+-$ events. Counter measurements of this reaction¹² have shown that at high energies, $d\sigma/dt$, where t is the square of the 4-momentum transfer to the proton, fits a smooth exponential dependence in t near $t=0$. By extrapolating our data it was estimated that short-proton-track losses are significant for $|t| < 0.06$ GeV^2 . This effect appears correlated with the number of pairs per frame (although apparently being independent of track orien-

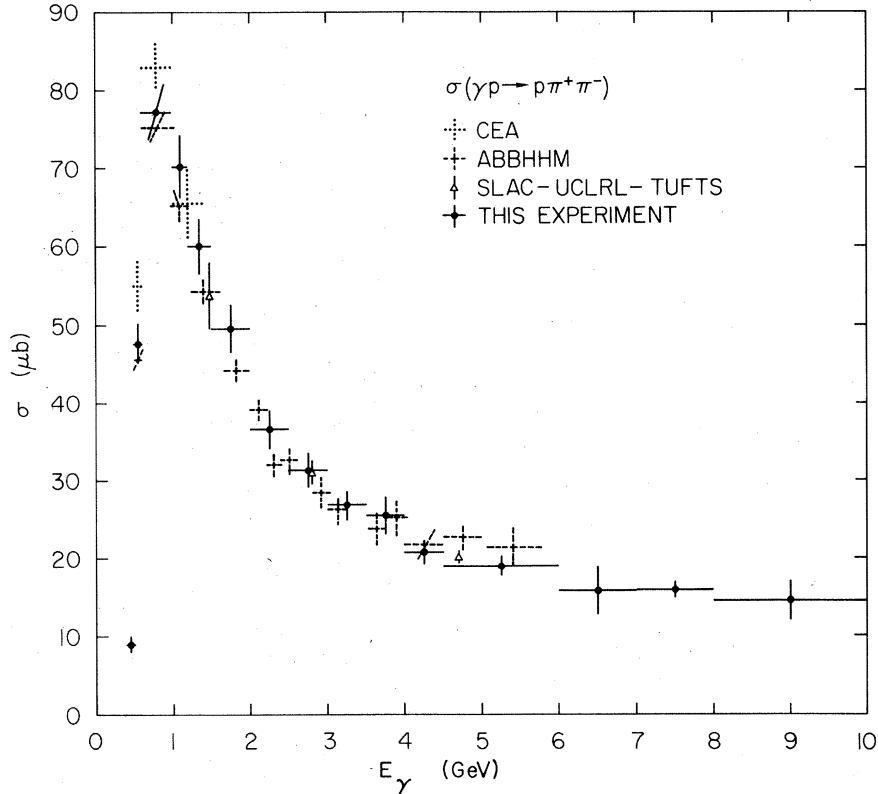


FIG. 3. Cross sections for the reaction $\gamma p \rightarrow p\pi^+\pi^-$, as a function of energy E_γ , found in this experiment, and compared with other determinations. Points marked CEA are from Ref. 1; ABBHBM, Ref. 2; SLAC-UCLRL-TUFTS, Ref. 6.

tation), and indicates a $\sim 13\%$ loss for photon energy > 4 GeV. At low energies the loss becomes less important.

Corrections due to effects (2)–(4) were all studied by using the track-measurement simulation program PHONY,¹³ which generates film-plane measurements, weighted by predetermined matrix elements, and subjected to multiple scattering, bremsstrahlung, nuclear interactions, and setting

error. It was found that such simulated events could reproduce the χ^2 distributions of actual fitted events, including a low-confidence-level peak presumably from the nuclear interactions along the tracks. In the case of pair measurements it was found that nearly 10% of photons in the peak

TABLE III. Cross sections for the 3C (3-constraint) fit reactions $\gamma p \rightarrow p\pi^+\pi^-$ and $\gamma p \rightarrow p\pi^+\pi^+\pi^-\pi^-$ found in this experiment, averaged in the energy intervals shown.

E_γ (GeV)	$\sigma(\gamma p \rightarrow p\pi^+\pi^-)$ (μb)	E_γ (GeV)	$\sigma(\gamma p \rightarrow p\pi^+\pi^+\pi^-\pi^-)$ (μb)
0.4–0.5	9.0 ± 1.0		
0.5–0.6	47.6 ± 3.0		
0.6–1.0	77.2 ± 3.5		
1.0–1.2	70.2 ± 4.0		
1.2–1.5	60.0 ± 3.5	1.2–1.5	0.035 ± 0.04
1.5–2.0	49.5 ± 3.0	1.5–2.0	0.8 ± 0.2
2.0–2.5	36.5 ± 2.0	2.0–2.5	1.9 ± 0.3
2.5–3.0	31.2 ± 2.2	2.5–3.0	3.1 ± 0.5
3.0–3.5	26.8 ± 2.0	3.0–4.0	5.5 ± 0.7
3.5–4.0	25.3 ± 2.5	4.0–5.0	4.4 ± 0.7
4.0–4.5	20.7 ± 2.0	5.0–5.5	4.9 ± 0.7
4.5–6.0	19.0 ± 1.0	5.5–6.0	6.0 ± 1.0
6.0–7.0	15.8 ± 2.0	6.0–7.0	4.6 ± 0.9
7.0–8.0	16.0 ± 1.2	7.0–8.0	4.6 ± 0.4
8.0–10.0	14.5 ± 2.5	8.0–10.0	5.4 ± 1.0

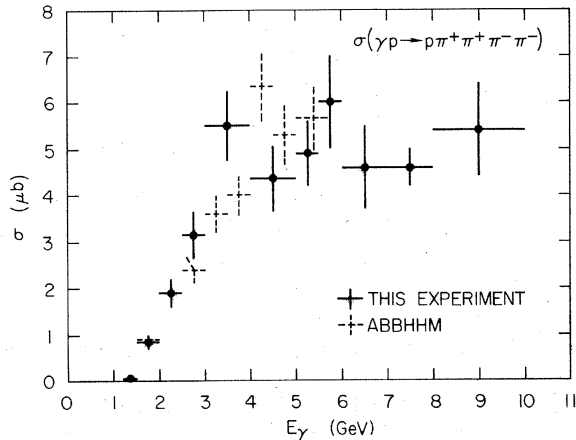


FIG. 4. Cross sections for the reaction $\gamma p \rightarrow p\pi^+\pi^+\pi^-\pi^-$ as function of energy. ABBHBM points are from Ref. 2.

would appear to have energies in the bremsstrahlung component of the beam.

The photon spectrum was obtained by an iteration: The energy spectrum of 3C, $p+-$ events was normalized by the ratio $\sigma(\text{pair})/\sigma(p+-)$, the PHONY pair spectrum was folded in, and the change in the content of each energy bin was used to correct the actual measured pair spectrum.

If N_m is the total number of pairs measured, ΔN_m the number of pairs of the corrected spectrum in the interval ΔE at energy E , we have for the flux e in events/ $\mu\text{b GeV}$

$$e(E) = \frac{\Delta N_m}{\Delta E} \frac{1}{N_m \sigma(\text{pair})} \sum_{i=1}^{N_{\text{roll}}} \Phi_i. \quad (5a)$$

Φ_i is the "pair flux" for roll i , defined as follows to account for changes in photon flux:

$$\Phi = \frac{(\text{number of pairs counted})}{(\text{number of pair frames})} \times (\text{number of good frames}). \quad (5b)$$

The spectra deduced by this method are shown in Figs. 1(b), 1(c), and 1(d).

The cross section for the 3C-fit reactions were found using the scanning, measuring, and forward loss corrections described. They are given in Table III and are shown in Figs. 3 and 4, along with previous determinations. Agreement is generally good, except that in the 5-GeV region, the pair-spectrum correction may be responsible for the ~ 1 -standard-deviation disagreement with the ABBHMM result.² Note also that the present cross sections represent a revision of our preliminary values.^{4,5}

In the case of the 1C-fit reactions, the following procedure was adopted to obtain the total channel cross sections. The "missing mass" was plotted for each event consistent by track ionization with the 1C hypothesis (ambiguous events given multiple entries) without regard to fits, as is shown in Fig. 2. The backgrounds expected from multineutral events and from wrong track identification were superimposed and assigned a "reasonable" error. Then events of the proper category were generated

TABLE IV. Cross sections found for the reactions $\gamma p \rightarrow p \pi^+ \pi^- \pi^0$ and $\gamma p \rightarrow n \pi^+ \pi^+ \pi^-$ at the annihilation peak energies, averaged over a photon energy interval of approximately 1 GeV.

E_γ (GeV)	$\sigma(\gamma p \rightarrow p \pi^+ \pi^- \pi^0)$ (μb)	$\sigma(\gamma p \rightarrow n \pi^+ \pi^+ \pi^-)$ (μb)
4.3	18.2 ± 2.0	7.5 ± 1.5
5.25	13.5 ± 1.5	4.6 ± 1.5
7.5	11.8 ± 1.2	4.0 ± 1.3

by PHONY, having a phase-space distribution weighted by the observed over-all momentum-transfer distribution to the nucleon and an incident photon energy given by the distributions of Fig. 1. These events were fitted by the complete TVGP system in a manner identical to that of the experimental sample and subjected to the cuts described in Sec. III, giving an efficiency for fitting both annihilation- and bremsstrahlung-induced events to the 1C hypothesis when subjected to the cuts described above. This factor was used to correct the number of events above the other backgrounds shown in Fig. 2 and finally the cross section for these events was found using Eq. (4), assuming no significant energy dependence over the energy interval involved. In the case of the channel $p+-0$ the ω was treated separately, but in a similar manner, and the forward loss correction factor found for the ρ meson was applied. The final values obtained for the 1C channels are given in Table IV, and shown, along with previous measurements, as a function of energy in Fig. 5.

V. THE REACTION $\gamma p \rightarrow p \pi^+ \pi^-$

A. General Features

This reaction has been investigated in previous track-chamber experiments^{1-3,6} and by counter techniques,¹² which showed that above $E_\gamma = 1.5$ GeV the reaction

$$\gamma p \rightarrow p \rho^0 \quad (6)$$

dominates the channel, having a roughly constant cross section, sharply peripheral production angular distribution, and being consistent with a natu-

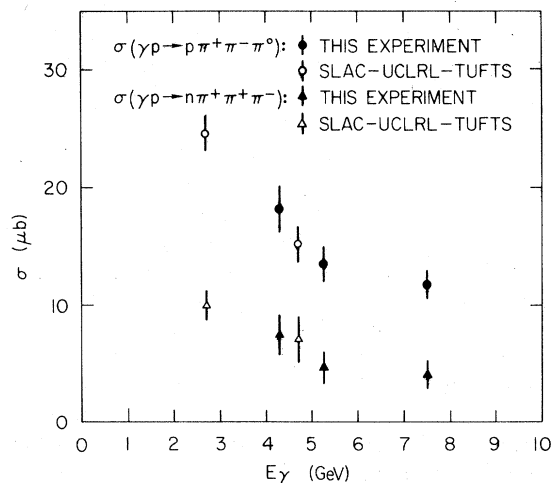


FIG. 5. Cross sections for a single neutral in the final state of the three-prong topology. SLAC-UCLRL-TUFTS points, see Ref. 35.

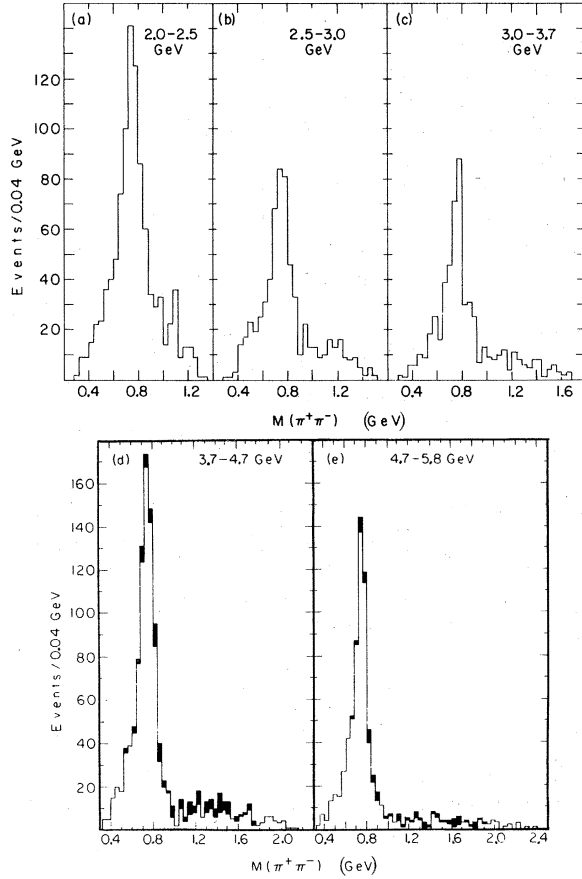


FIG. 6. Dipion mass distributions for $\gamma p \rightarrow p \pi^+ \pi^-$ for the first five energy intervals as labeled. The darkened areas of (d) and (e) represent events with $p\pi$ mass in the $\Delta(1236)$ region [$1.12 < M_{p\pi} < 1.35$ GeV and $|t(p, \Delta)| < 0.8$ GeV²].

ral-parity t -channel exchange mechanism.^{6,14} These observations have led to the interpretation of this reaction as a diffractive process. For squared momentum transfer to the proton, $|t|$, less than 0.4 GeV², it appears that s -channel helicity is conserved at the photon vertex.^{6,15} In addition a contribution $\sim E_\gamma^{-2}$ from the reaction^{1,2,8,16}



is observed. Evidence has been sought, but not found, for resonances other than ρ^0 in the $\pi^+ \pi^-$ -mass system.¹⁷ In this section we confirm some of these features in our data, add data at higher energies, and confirm that reaction (6) increasingly dominates the channel as incident energy increases.

It is important to point out here that in the bubble chamber we are free of possible backgrounds from reactions other than $\gamma p \rightarrow p \pi^+ \pi^-$. As will be shown later there is considerable ρ^0 production in other reactions which might be hard to eliminate with other techniques.

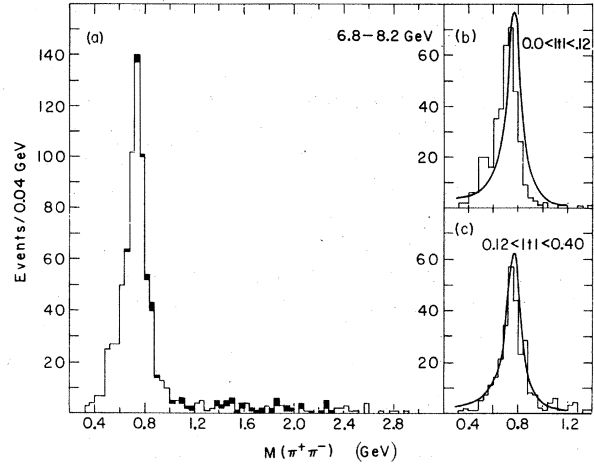


FIG. 7. Dipion mass distributions for $\gamma p \rightarrow p \pi^+ \pi^-$ in the photon energy range 6.8–8.2 GeV. (a) All events. Darkened areas represent events with Δ , as in previous figure; (b) same distribution for events with $0 < |t| < 0.12$ GeV²; (c) same for $0.12 < |t| < 0.40$ GeV². The curves in (b) and (c) represent the same relativistic BW resonance [Eq. (9a)] with $m_\rho = 0.765$ GeV and fixed $\Gamma = 0.14$ GeV.

B. ρ^0 Production

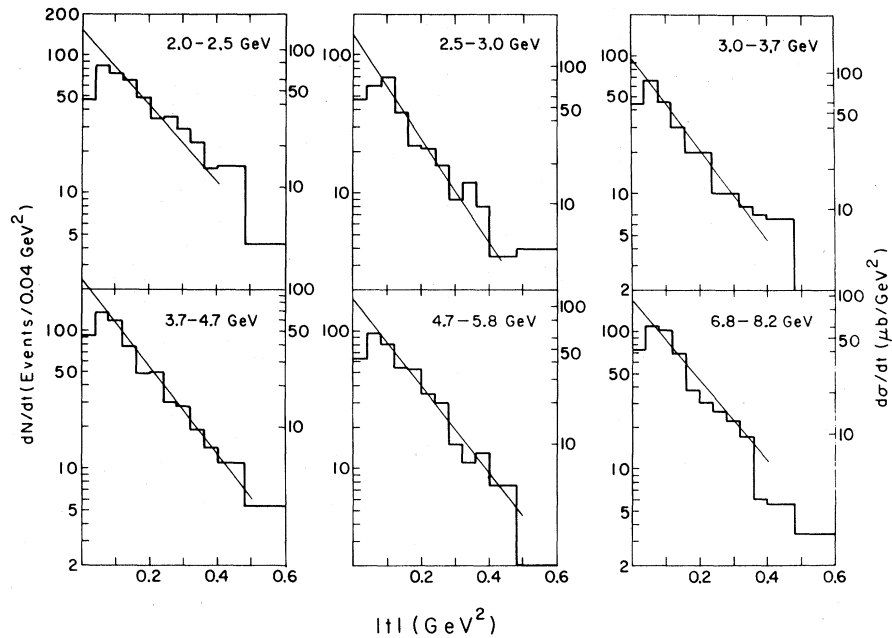
In Figs. 6(a)–6(e) and Fig. 7(a) the invariant mass of the $\pi^+ \pi^-$ system is shown for six photon-energy regions. The previously observed skewed distribution of the ρ^0 with respect to the usual Breit-Wigner (BW) shape becomes especially dramatic in the 7.5-GeV region (Fig. 7), there being essentially no sign of the high-mass tail to the distribution.¹⁸ In Figs. 7(b) and 7(c) the change of shape for the 7.5-GeV data with t is illustrated by plotting the distribution near the ρ^0 mass for $0 \leq |t| \leq 0.12$ GeV² and $0.12 \leq |t| \leq 0.4$ GeV². At large $|t|$ the mass distribution can be qualitatively described by a relativistic Breit-Wigner form [Eq. (9a) below] with fixed Γ as is shown by the solid curve on both distributions, but at small t the high-mass tail is significantly below even the s -wave BW prediction. This distortion means that a full analysis must depend upon the production model adopted. In the following we use procedures parallel to those of the Stanford-Berkeley-Tufts (SBT) collaboration⁶ and shall note any differences in approach.

To present the raw data independent of models we begin with a purely phenomenological approach. We assume that the double differential cross section for dipion production with $|t| < 0.4$ GeV² may be described by the form

$$\frac{d^2\sigma}{dt dm} = A e^{Bt}, \quad (8)$$

where A and B are functions of m , the dipion in-

FIG. 8. $|t|$ distributions for events in the ρ^0 region ($0.60 < m < 0.85$ GeV) for various E_γ intervals. The right-hand side scale and the curves represent $d\sigma/dt$ for the phenomenological fit (Table VI).



variant mass. In Fig. 8 we show the t distributions for events with m in the ρ^0 region ($0.60 < m < 0.85$ GeV), which show that Eq. (8) represents this region well ($d\sigma/dt$ values will be presented later). The loss in scanning of events at small t , mentioned earlier, is evident here. We determined A and B for fixed intervals in m for events with $0.06 < |t| < 0.4$ GeV² using a maximum-likelihood method. The resulting forward cross sections and slopes are shown in Fig. 9. The variation of slope with mass becomes more marked at the highest energies but is consistent with the same value at the ρ^0 mass: $B(0.715 < m < 0.815$ GeV) = 7.1 ± 0.4 GeV⁻² for $3.7 < E_\gamma < 8.2$ GeV, statistically in agreement with that of the SBT collaboration⁶ which finds (6.8 ± 0.5) GeV⁻² for $E_\gamma = 4.7$ GeV.

We now make the observation that the production models suggested in the literature fall into two classes: (1) *the interference model* of Söding¹⁹ and (2) *kinematic skewing or phenomenological models*, such as suggested, e.g., by Ross and Stodolsky, by Kramer and Uretsky, and by Mannheim and Maor.²⁰ In the first class we would include also models differing from that of Söding in the details of the interfering background,¹⁹ in the second any modifications of the kinematic factor, e.g., as used in Ref. 6. We have chosen a particular example of each class to provide functional forms describing the dipion production data and by fitting these have obtained ρ^0 cross sections and values for the mass and width of the ρ^0 . Applied to the same data these values differ by small amounts which may be regarded as a measure of the theoretical uncertainties inherent in the model

approach. A third set of cross sections were derived from the intensity of dipion pair production near the ρ^0 mass in a manner described below. These latter values are the least model-dependent within our present theoretical understanding. We therefore have three ρ^0 photoproduction cross sections which will be termed (a) Söding-fit values, (b) phenomenological values, and (c) values obtained by the "standard" method. The true ρ^0 cross sections presumably lie somewhere within the range of these values. We now describe our procedures.

(a) *Söding fits*. As has been shown at lower energies^{2,6} the characteristics of ρ^0 photoproduction are well described by the Söding interference model.¹⁹ In this model the distorted ρ^0 shape is due to an interference of a diffractively produced ρ^0 [shown as a Feynman graph in Fig. 10(a)] with a p -wave $\pi\pi$ background from a Drell diagram²¹ [Figs. 10(b), 10(c)]. It was shown in Ref. 6 that this model explains most features of ρ^0 production at 2.8 and 4.7 GeV including the skewing of the mass distribution and its variation with t . If M_1 , M_2 , and M_3 are the matrix elements for the diagrams in Figs. 10(a), 10(b), and 10(c) then the cross sections for diffractive ρ^0 production, the "Drell term," and the interference term are given by $|M_1|^2$, $|M_2 + M_3|^2$, and $2 \text{Re}[M_1^*(M_2 + M_3)]$, respectively. In the calculations, the explicit formulas given in Ref. 19 for M_1 , M_2 , and M_3 were used with the following changes (Appendix B, last paper, Ref. 6): (1) We used $M_1 \propto \exp(\frac{1}{2}B^{\text{Söding}} t)$ to describe the t dependence of ρ^0 diffractive production. (2) The amplitudes $T_{\pm}(s, t)$ which describe

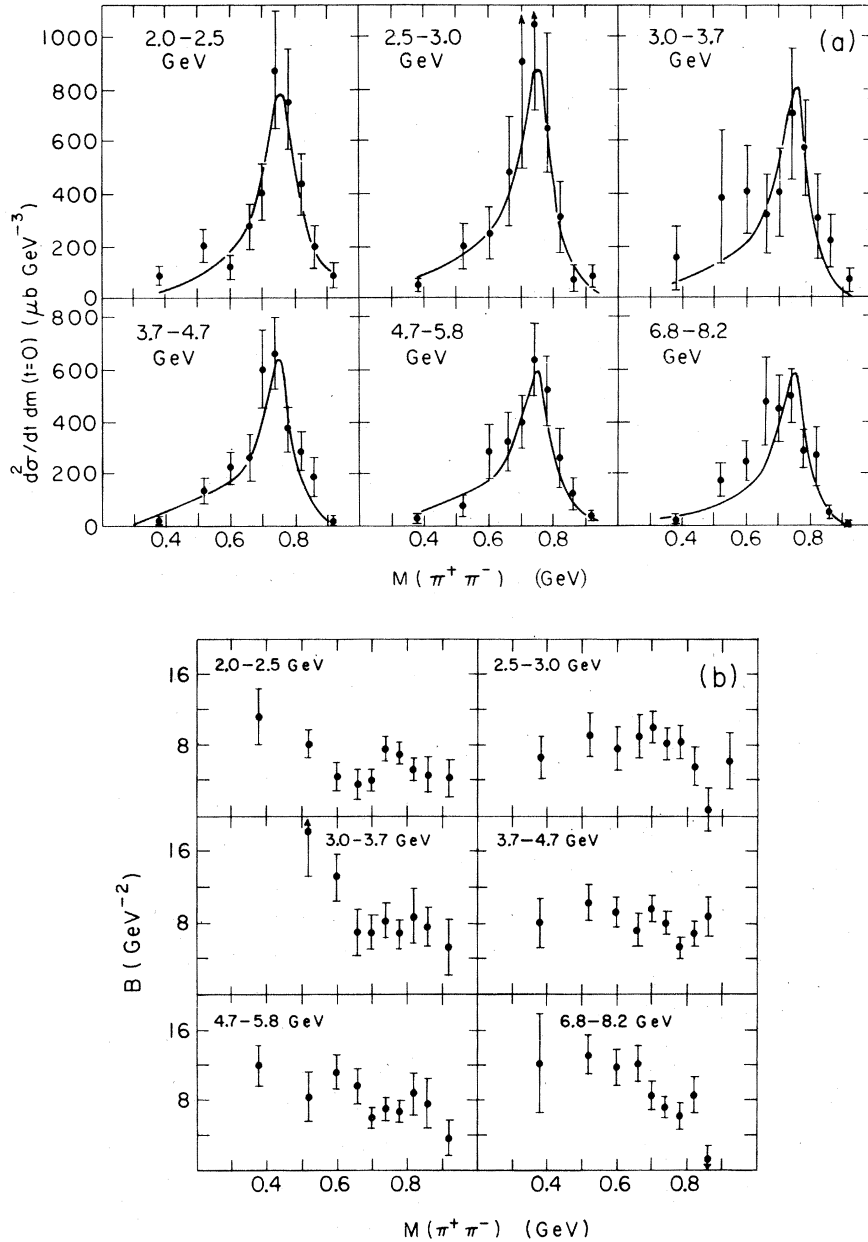


FIG. 9. (a) Double-differential cross section $d^2\sigma/dt dm(t=0)$. As illustration we show the phenomenological fits to the data [Eq. (9) with $\Gamma_0=0.125$ GeV, $m_\rho=0.765$ GeV]. The exponent $n=6$ was used at all energies except $E_\gamma=2.0-2.5$ GeV, where $n=4$ gave a better fit. (b) The slope B for the interval $0.06 \leq |t| \leq 0.40$ GeV² as a function of the dipion mass.

the πN interaction at the lower vertex were evaluated from the πN phase-shift data for $M_{\pi p} < 1.74$ GeV. The virtual nature of the interacting pion was accounted for by multiplying the amplitudes $T_{\pm}(s, t)$ by a Ferrari-Selleri-type form factor.²² (3) Double counting was avoided by introducing corrections for the rescattering of the dipion system to form a ρ^0 indistinguishable from that directly produced. This can be done by multiplying the

Drell matrix element by $e^{i\delta} \cos\delta$ where δ is the p -wave phase shift associated with the ρ^0 resonance in elastic $\pi\pi$ scattering.²³ To evaluate the total ρ^0 cross section, the events in reaction (1) were fitted to an incoherent sum of three distributions given by: (a) the diagrams of Figs. 10(a)–10(c) with rescattering corrections, allowing the ρ^0 mass, width, and t slope, $B^{\text{S}d}$, in M_1 to be free parameters determined by the fitting program, (b)

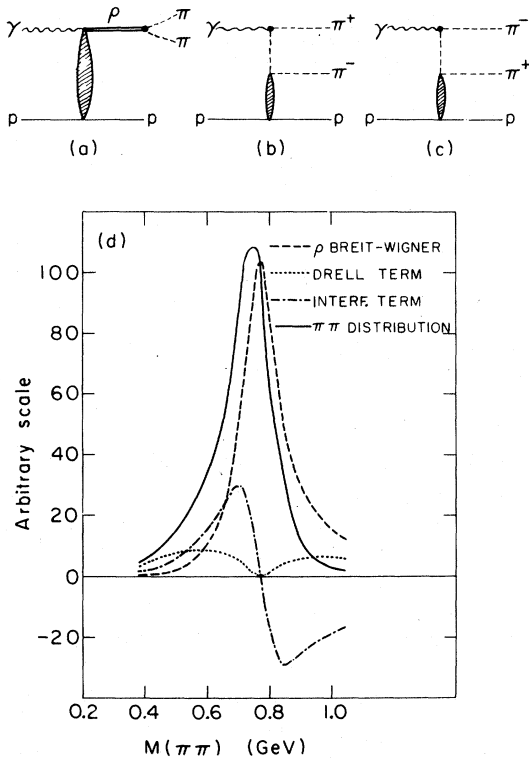


FIG. 10. (a)–(c) The contributing diagrams in the Soding model. (d) The contributions of the Drell, interference, and p -wave Breit-Wigner terms to the $\gamma p \rightarrow p \pi^+ \pi^-$ cross sections at 7.5 GeV. The distributions are normalized to the number of the Drell, interference, and ρ^0 events obtained with the Soding fit.

the reaction $\gamma p \rightarrow \Delta^{++} \pi^-$, and (c) Lorentz-invariant phase space. The cross section for $\gamma p \rightarrow \rho^0 p$ was taken to be $|M_1|^2$ while the $|M_2 + M_3|^2$ and the interference terms were regarded as background. In Fig. 10(d) we show the projected dipion mass distribution of the ρ , Drell background, and interference terms, indicating their relative importance for the 7.5-GeV data.

The parameters M_ρ , Γ_ρ , and $B^{\text{Söd}}$ of the Soding

model were determined from a fit in the t region $|t_1| = 0.06 < |t| < |t_2| = 0.4 \text{ GeV}^2$. The cross section for ρ^0 events in this t range, $\sigma_\rho(t_1, t_2)$, was then increased by the ratio of $|M_1|^2$ integrated over the entire physical region of phase space to $|M_1|^2$ integrated over the above restricted t range in order to obtain the total ρ^0 cross section.

The forward ρ^0 cross section was computed from $\sigma_\rho(t_1, t_2)$ by extrapolating to $t=0$ using

$$\frac{d\sigma^{\text{Söd}}}{dt}(t=0) = \frac{B^{\text{Söd}} \sigma_\rho(t_1, t_2)}{\exp(B^{\text{Söd}} t_1) - \exp(B^{\text{Söd}} t_2)}.$$

In this way we avoid the effects of scanning losses at small t and the distortion by the kinematic boundary at t_{\min} , the minimum squared 4-momentum transfer. The resulting fit parameters and cross sections are given in Tables V and VI.

(b) *Phenomenological fits.* Here the ρ^0 shape was parametrized by⁶:

$$P(m) = \left(\frac{m_\rho}{m}\right)^{n(t)} f(m) L(m), \quad (9a)$$

$$f(m) = \frac{\Gamma(m)}{(m_\rho^2 - m^2)^2 + m_\rho^2 \Gamma^2(m)}, \quad (9b)$$

$$\Gamma(m) = \left(\frac{q}{q_\rho}\right)^3 \frac{2q_\rho^2}{q_\rho^2 + q^2} \Gamma_\rho. \quad (9c)$$

$L(m)$ is a Lorentz-invariant two-body phase-space factor, q and q_ρ are the π momenta in the dipion rest frame for dipion masses of m and m_ρ , respectively, and Γ_ρ is the ρ width. Equation (9a) is essentially the Ross-Stodolsky²⁰ form, where the constant exponent is replaced by a t -dependent exponent $n(t)$. This parametrization, first used in Ref. 6, describes well the experimental data. When fitted over the full range of t we get $\langle n(t) \rangle \approx 4$ at all energies. However, when the fit is repeated for distinct t intervals $n(t)$ is found to be a function of t , decreasing from about 5.5 at $0 \leq |t| \leq 0.12 \text{ GeV}^2$ to near zero at large t , in agreement with the results of Ref. 6. As in the Soding fits, we have

TABLE V. Fitted masses, widths, and total cross sections for ρ^0 produced in $\gamma p \rightarrow \rho^0 p$ as obtained by the Soding and phenomenological fits made in the interval $0.06 < |t| < 0.4 \text{ GeV}^2$. Cross sections are corrected for other t values assuming a linear exponential.

E_γ (GeV)	Events		Phenomenological			Soding		
	Uncorrected	Corrected	m_ρ (MeV)	Γ_0 (MeV)	σ_ρ (μb)	m_ρ (MeV)	Γ_0 (MeV)	σ_ρ (μb)
2.0–2.5	1001	1001	769 ± 6	144 ± 14	22.1 ± 1.4	764 ± 7	143 ± 12	19.1 ± 1.7
2.5–3.0	642	642	772 ± 6	136 ± 15	21.4 ± 1.6	765 ± 8	146 ± 15	18.5 ± 1.9
3.0–3.7	552	588	772 ± 7	141 ± 18	18.7 ± 1.6	773 ± 8	140 ± 15	15.7 ± 1.7
3.7–4.7	775	852	769 ± 6	134 ± 10	16.2 ± 1.7	774 ± 5	142 ± 10	14.7 ± 1.7
4.7–5.8	536	606	759 ± 4	110 ± 10	15.4 ± 1.4	754 ± 5	122 ± 12	16.6 ± 1.7
6.8–8.2	809	917	758 ± 5	151 ± 11	13.7 ± 1.3	771 ± 6	147 ± 10	14.3 ± 1.3

TABLE VI. Forward cross sections and slopes for the ρ^0 as obtained by the three methods, and forward-double differential cross sections for $m_{\pi\pi}=0.715-0.815$ GeV. Slopes B were determined in the range $0.06 \leq |t| \leq 0.4$ GeV².

E_γ (GeV)	$\frac{d\sigma}{dt}(t=0)$ ($\mu\text{b GeV}^{-2}$)			B (GeV ⁻²)			$\left\langle \frac{d^2\sigma}{dt dm}(t=0) \right\rangle$ $m_{\pi\pi}=0.715-0.815$ GeV ($\mu\text{b GeV}^{-3}$) ^a
	Phenom.	Söding	Standard ^a	Phenom.	Söding	Standard ^a	
2.0-2.5	138 ± 20	143 ± 14	180 ± 20	5.9 ± 0.7	5.4 ± 0.5	6.7 ± 0.9	770 ± 90
2.5-3.0	179 ± 27	170 ± 17	184 ± 25	7.7 ± 0.9	6.4 ± 0.6	7.5 ± 1.1	780 ± 110
3.0-3.7	159 ± 26	160 ± 16	152 ± 22	8.2 ± 1.0	7.1 ± 0.7	7.5 ± 1.2	650 ± 100
3.7-4.7	130 ± 13	100 ± 10	105 ± 10	7.5 ± 0.6	6.5 ± 0.5	6.8 ± 0.7	450 ± 45
4.7-5.8	123 ± 14	132 ± 13	117 ± 12	7.6 ± 0.6	7.7 ± 0.6	6.7 ± 0.8	500 ± 55
6.8-8.2	104 ± 11	102 ± 10	90 ± 10	7.5 ± 0.6	7.1 ± 0.6	7.0 ± 0.8	380 ± 40

^a No incoherent-background correction.

also allowed contributions from the reaction $\gamma p \rightarrow \Delta^{++} \pi^-$ and from Lorentz-invariant phase space. The fractions of $p\rho^0$, $\Delta^{++} \pi^-$, and Lorentz-invariant phase space were fitted together with the ρ^0 mass, width, and $\langle n(t) \rangle$. The ρ^0 slope and forward cross section were derived by repeating the fit in t intervals and fitting the resulting ρ^0 cross sections to the exponential form (8) in the range $0.06 \leq |t| \leq 0.40$ GeV². This fit to the differential cross section was also used to correct the total phenomenological ρ^0 cross section for $|t_{\min}| \leq |t| \leq 0.06$ GeV². Tables V and VI list the values found.

(c) "Standard" method. Yennie²³ has pointed out that in the absence of incoherent background processes, the Söding model predicts that the values of $d^2\sigma/dt dm$ at $m=m_\rho$ is given to good approximation by the peak of the Breit-Wigner resonance shape describing an undistorted ρ^0 meson. This is because the p -wave of the Drell and interference terms vanish here and contributions from other partial waves are small. Hence by multiplying $d^2\sigma/dt dm$ ($m=m_\rho$) by a factor

$$F = \int f(m) dm^2 / 2m_\rho f(m_\rho), \quad (10)$$

where $f(m)$ is defined in Eq. (9b), we can derive a ρ^0 cross section which is independent of details of the skewing mechanism. However, this method

provides no estimate of incoherent background and therefore will only be reliable for our data at the higher energies where such background is found to be small by the previous fitting procedures.

To obtain the slope and forward differential cross sections we fitted Eq. (8) to our data in the range $0.715 < m < 0.815$ GeV and $0.06 < |t| < 0.4$ GeV² to obtain the averaged double-differential forward cross section $\langle d^2\sigma/dt dm \rangle$ at $t=0$. The values found are given in the last column of Table VI. To obtain $d^2\sigma/dt dm$ ($t=0, m=m_\rho$), we corrected the average values by a factor,

$$f(m_\rho) / \langle f(m) \rangle_{0.715 < m < 0.815 \text{ GeV}} = 1.15, \quad (11)$$

derived from Eq. (9b) for $\Gamma_\rho = 0.130$ GeV. Because of the narrow mass interval chosen, this factor changes insignificantly for Γ_ρ in the range 0.12-0.15 GeV. Since the true ρ^0 shape is not well known, we use the zero-width limit of the Breit-Wigner form and choose $F = \frac{1}{2} \pi \Gamma_\rho$ with $\Gamma_\rho = 130$ MeV, as suggested by Yennie.²³ The prescription becomes

$$\frac{d\sigma^{\text{Stand}}}{dt}(t=0) = 1.15 \left\langle \frac{d^2\sigma}{dt dm} \right\rangle \frac{\pi \Gamma_\rho}{2}. \quad (12)$$

These values are shown in Table VI. Uncertainties

TABLE VII. Event distribution for the reaction $\gamma p \rightarrow p \pi^+ \pi^-$ in the mass range $M(\pi^+ \pi^-) = 0.715-0.815$ GeV. The corresponding cross sections are from the "standard" method described in the text.

t (GeV ²)	4.3 GeV		5.25 GeV		7.5 GeV	
	Events	$d\sigma/dt$ ($\mu\text{b/GeV}^2$)	Events	$d\sigma/dt$ ($\mu\text{b/GeV}^2$)	Events	$d\sigma/dt$ ($\mu\text{b/GeV}^2$)
0.06-0.10	71	65 ± 7	52	69 ± 9	44	45 ± 6
0.10-0.15	60	44 ± 5	48	51 ± 7	55	44 ± 6
0.15-0.20	42	31 ± 4	40	43 ± 6	31	25 ± 4
0.20-0.30	53	19 ± 2.5	38	20 ± 3	40	16 ± 2
0.30-0.40	31	11 ± 2	21	11 ± 2	19	7.7 ± 1.7
0.40-0.80	32	2.9 ± 0.5	25	3.3 ± 0.6	18	1.8 ± 0.4

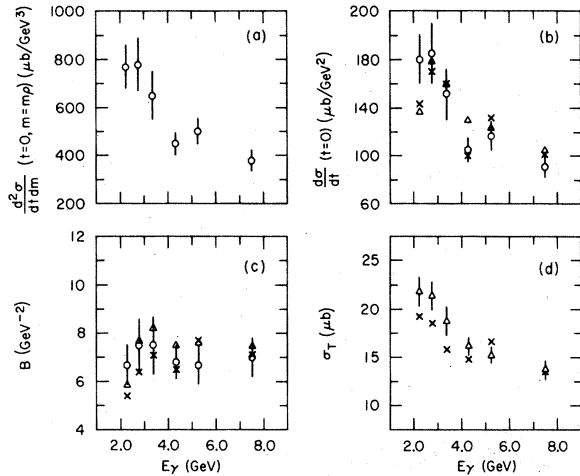


FIG. 11. (a) Average double-differential forward cross sections near the ρ^0 mass ($m_{\pi\pi} = 0.715\text{--}0.815$ GeV). (b) Forward differential cross sections and (c) slopes determined in the three methods (see text). (d) Total ρ^0 cross sections. The results are given for the standard (circles), phenomenological (triangles), and Söding (crosses) methods. The errors are those obtained in the standard fits (a)–(c) and phenomenological fits (d).

resulting from the values chosen for the central mass and width of the ρ^0 meson are not included in our errors.

In similar fashion we have determined $d\sigma_p/dt$ in finite t bins. These are shown for $E_\gamma > 3.7$ GeV in Table VII, along with the actual numbers of events

used to determine $\langle d^2\sigma/dt dm \rangle$.

The results obtained by the three methods are summarized in Tables V, VI, VII, and Fig. 11. It appears that at high energies all three approaches yield similar results within errors.

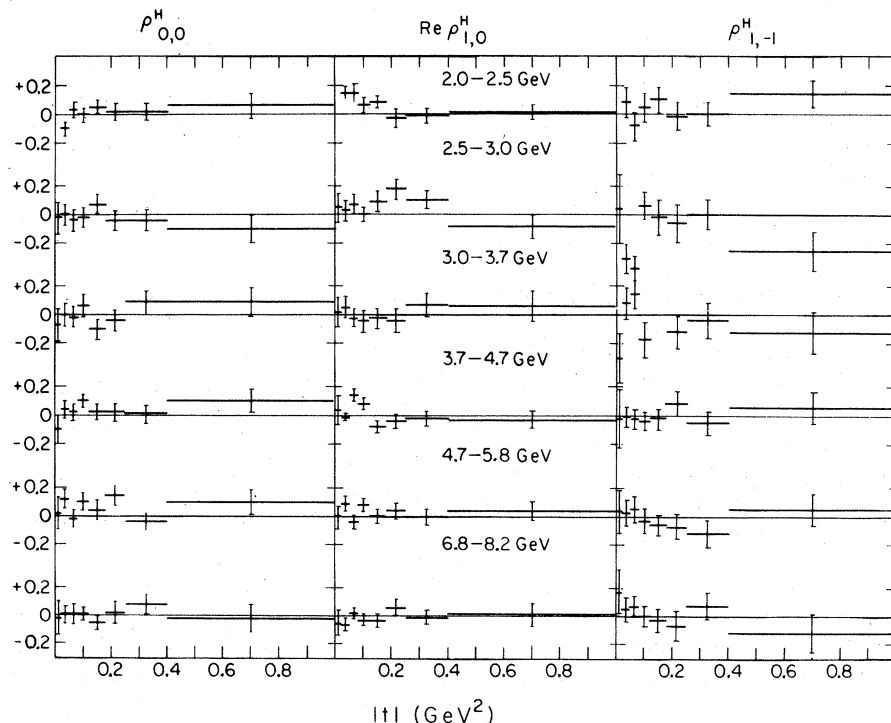
One should note (see Table V) that the fitted mass and width of the ρ^0 are about 0.765 GeV and 0.135 GeV respectively, and seem to be independent of the photon energy, in both the Söding and phenomenological methods.

The dipion slope near the ρ^0 mass is consistent with about 7 GeV^{-2} for $3 \leq E_\gamma \leq 8$ GeV and similar slopes are obtained from the Söding and phenomenological fits [see Fig. 11(c)]. The forward cross sections from all three methods drop slowly with increasing photon energy, as has been observed previously.^{2,17}

Comparing to counter experiments of ρ^0 photoproduction¹⁷ we find that our average slope B is smaller than that observed in most counter measurements and closer to the Compton-scattering slopes.²⁴ Moreover, the forward cross sections, reported here, seem to be slightly lower. These discrepancies may be caused in part by a contamination from inelastically produced ρ^0 mesons in the counter experiments or by a change in the slope of ρ^0 photoproduction for $|t| < 0.06 \text{ GeV}^2$.

The results from the phenomenological method can be compared to those of other bubble-chamber experiments.^{2,6} Total and forward cross sections as well as the slope of the differential cross sec-

FIG. 12. Spin-one density-matrix elements in the helicity frame for the dipion system in the ρ^0 region ($0.60 < m < 0.85$ GeV) with background subtraction.



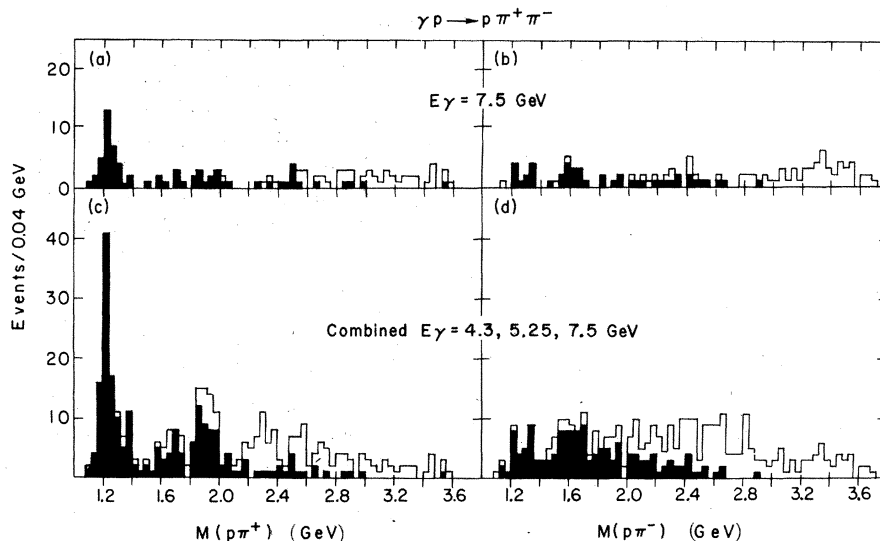


FIG. 13. (a) $M(p\pi^+)$ and (b) $M(p\pi^-)$ distributions for $\gamma p \rightarrow p\pi^+\pi^-$ events with $M(\pi^+\pi^-) > 1$ GeV ($E_\gamma = 7.5$ GeV). The solid areas correspond to events with $|t(p, p\pi^+)| < |t(p, p\pi^-)|$ in (a) and to $|t(p, p\pi^-)| < |t(p, p\pi^+)|$ in (b). (c) and (d) are the same distributions as in (a) and (b) for the combined data of the 4.3-, 5.25-, and 7.5-GeV experiments.

tion agree at corresponding energies. The Söding model is applied here in a way slightly different from that used by the SBT collaboration.⁶ The total cross sections were fitted in both experiments by equivalent methods and indeed they agree. The slope $B^{\text{Söding}}$ in the present work was fitted directly in the ρ^0 matrix element, while the SBT collaboration⁶ determined it from a fit to the differential ρ^0 cross sections. Thus the kinematic cutoff at large $M_{\pi\pi}$ and small t brings about the smaller slopes found by SBT. We further remark that since the Söding model describes the data very well, our procedure for deriving the forward Söding cross section is essentially equivalent to the standard method, using a ρ^0 width which would fit the observed $\pi^+\pi^-$ mass distribution. However, the Söding-model fits subtract the incoherent background which is of increasing importance as E_γ decreases. Figure 11(b) indeed shows that the values of the forward cross sections from the standard method are higher at low E_γ .

Using the method of moments, we have determined the spin-one density-matrix elements for the dipion system in the ρ^0 region (0.6–0.85 GeV). As has been observed previously^{2,6} the helicity system provides the simplest description of the distribution because the helicity of the photon appears to be conserved. In Fig. 12 we show the behavior of the three measurable elements ρ_{00} , $\text{Re}\rho_{10}$, and ρ_{1-1} in the helicity system.²⁵ Background from Δ^{++} reflections and phase space was subtracted by analyzing with and without Δ^{++} cuts and interpolating. For most points, and in particular in the small- $|t|$ regions, the corrections

were negligible. The γ - ρ helicity-conservation hypothesis⁶ (no helicity flip in the s -channel helicity system) is compatible with the data up to $|t| = 0.4$ GeV² and at 7.5 GeV may be good up to $|t| = 1.0$ GeV².

C. Nucleon Resonances

In addition to the ρ^0 production we observe Δ in reaction (7) at all energies. Figure 13(a) shows

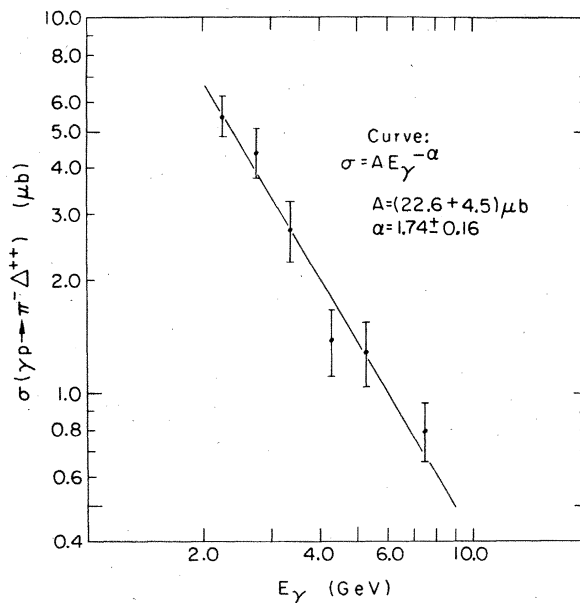


FIG. 14. Cross sections for $\gamma p \rightarrow \Delta^{++}\pi^-$ as obtained with a fit to a relativistic p -wave Breit-Wigner form for the Δ . The solid line represents the best fit to the form $A E_\gamma^{-\alpha}$.

the $M(p\pi^+)$ spectrum for events with $M(\pi^+\pi^-) > 1$ GeV in the 7.5 GeV data where $\Delta^{++}\pi^-$ production is apparent. Events for which the squared momentum transfer between the target proton and the final $p\pi^+$, $t(p, p\pi^+)$, is smaller than $t(p, p\pi^-)$ are shaded. For a nucleon isobar produced by a peripheral mechanism, one would expect the smaller of the t values to be associated with the isobar, as is clearly true for $\Delta^{++}(1236)$. Figure 13(b) shows a similar plot with the π^+ replaced by the π^- . In Figs. 13(c) and 13(d) we show the combined data for the 4.3-, 5.25-, and 7.5-GeV regions for $M(p\pi^+)$ and $M(p\pi^-)$, respectively, using events with $M(\pi^+\pi^-) > 1$ GeV. The solidly blocked events are those with the lesser momentum transfer. Although not statistically compelling, the accumulation of events in the 1.9-GeV region for $p\pi^+$ and the 1.6-GeV region for $p\pi^-$ indicate that a substantial fraction of events with $M(\pi^+\pi^-) > 1$ GeV may be accounted for by πN^* production (e.g., by the Drell process).

In Fig. 14 we show the cross sections for $\gamma p \rightarrow \pi^- \Delta^{++}$ at the six energies as determined from the phenomenological fits and using a relativistic p -wave shape, Eq. (9b) above, for the Δ^{++} . Our measurements agree with those of earlier experiments.^{1,2,16} The energy dependence of the Δ cross section is well described by $\sigma(\gamma p \rightarrow \pi^- \Delta^{++}) = A E_\gamma^{-\alpha}$ with a slope $\alpha = 1.74 \pm 0.16$ which is close to the slope for quasi-two-body hadron collisions produced by nonstrange-meson exchanges.²⁶ The use of a Δ shape other than Eq. (9b) (e.g., that used in Ref. 8) may reduce the magnitude of the cross section but will not change appreciably the slope α . If Δ production proceeds by pure OPE (one-pion exchange) one would expect $\rho_{11}^J = 0.5$ ($\rho_{33}^J = 0.0$) in the Jackson system²⁷ for the Δ decay. It is, however, difficult to draw decisive conclusions about the $\gamma p \rightarrow \pi \Delta$ production mechanism because of the small statistics involved and the reflections from the ρ^0 events. For the 7.5-GeV events with $|t(p, \Delta^{++})| \leq 0.4$ GeV² where the ρ^0 reflections are minimal (see Fig. 7) we find $\rho_{11}^J = 0.21 \pm 0.10$ in contradiction with the prediction of pure OPE without absorption. At 4.7 GeV, the polarized-photon experiment gave a similar conclusion.⁸

D. Higher-Mass Vector-Meson Production (ρ')

Vector mesons with the square of their mass forming a series with interval ~ 1 GeV² are predicted by the Veneziano model,²⁸ with decay width uncertain, but presumably allowed to decay to two pions. Also, some discrepancies between VDM (vector-dominance model) and experimental data could be reconciled by the existence of higher-mass vector mesons (see Sec. VII). No evidence

for such states is to be found in the spectra of Figs. 6 and 7. For the 7.5-GeV data the number of events with $m_{\pi\pi} > 1.0$ GeV turns out to be especially small. Furthermore, as was shown in the last paragraph a large fraction of these events may correspond to πN^* interactions. In Figs. 15(a) and 15(b) we present the angular distribution of the π^+ in the dipion helicity system for events with dipion mass > 1 GeV, and for two $t'(\gamma, \pi\pi)$ intervals ($t' = t - t_{\min}$ and t_{\min} is the minimum momentum transfer squared for the given dipion mass). The shaded events have an associated Δ . If the ρ' is diffractively produced in a c.m. helicity-conserving interaction ($\sin^2 \theta_\pi^H$ decay distribution) one would expect most of the ρ' to be at small t and to decay with $|\cos \theta_\pi^H| < 0.5$. In Fig. 15(c) we show the dipion mass distribution for events with $|\cos \theta_\pi^H| < 0.5$, where the shaded areas correspond to events with $|t'(\gamma \rightarrow \pi\pi)| < 0.4$ GeV². In the small- t sample we find about one event per 100 MeV in the 1650-MeV region and four events per 100 MeV near 1250 MeV, corresponding at the 90% confidence level to $\sigma_{\rho'}(1650) \leq 0.1$ μb and $\sigma_{\rho'}(1250) \leq 0.3$ μb per 100-MeV width of such resonances. These cross-section limits are for $|t'(\gamma \rightarrow \pi\pi)| < 0.4$ GeV² and include corrections for events with $|\cos \theta_\pi^H| > 0.5$ assuming

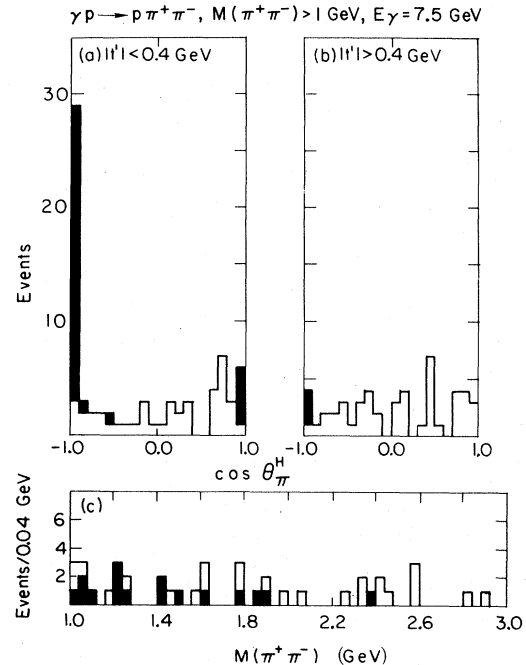


FIG. 15. (a), (b) Angular distributions of the π^+ in the helicity frame of the dipion system for events with $M(\pi^+\pi^-) > 1$ GeV for the 7.5-GeV data. Solid area represents Δ events. (c) Dipion mass distributions for those events with $|\cos \theta_\pi^H| < 0.5$. The solid area represents events with $|t'(\gamma, \pi\pi)| < 0.4$ GeV².

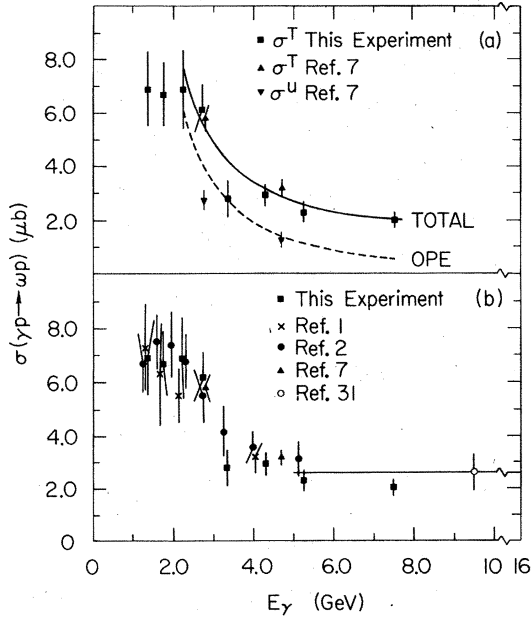


FIG. 16. (a) $\gamma p \rightarrow \omega p$ total cross sections measured in this experiment and in Ref. 7. σ^u is the unnatural-parity-exchange cross section for $|t| \leq 1.0 \text{ GeV}^2$ at 2.8 and 4.7 GeV (Ref. 7). The curves are best fits to Eq. (16) for $\alpha_1 = 2.0$ and $\alpha_2 = 0$ (see text). (b) Compilation of $\gamma p \rightarrow \omega p$ cross sections (Refs. 1, 2, 7, 31, and this experiment).

a $\sin^2 \theta_\pi^H$ distribution in the dipion system. Correction for high-momentum-transfer events are expected to be small if the t slope of the dipion system is comparable to that of the $\rho(765)$.

VI. THE REACTIONS $\gamma p \rightarrow N\pi\pi$

A. General

Unlike the channel $\gamma p \rightarrow p\pi^+\pi^-$ discussed in Sec. V, the 1C reactions

$$\gamma p \rightarrow p\pi^+\pi^-\pi^0, \quad (13a)$$

$$\gamma p \rightarrow n\pi^+\pi^+\pi^- \quad (13b)$$

are much more complex and difficult to analyze. The total cross section and the energy dependence for reactions (13) are given in Table IV and Fig. 5 above. In this section we shall discuss the quasi-two-body reactions

$$\gamma p \rightarrow \omega p, \quad (14a)$$

$$\gamma p \rightarrow \rho^-\Delta^{++}, \quad (14b)$$

$$\gamma p \rightarrow A_2^+n, \quad (14c)$$

and the inelastic ρ production

$$\gamma p \rightarrow \rho\pi N. \quad (14d)$$

Our detailed investigation of reactions (14a) and (14b) is presented in two recent publications^{29,30} but, for the sake of completeness, we shall summarize here briefly the main results concerning the two reactions.

B. ω Production

The ω is clearly seen at all energies between 1.2 and 8.2 GeV and is well separated from the background, especially at the high-energy regions. The ω -production cross sections, as observed in the present experiment are shown in Fig. 16(a). In Fig. 16(b) we show the results of earlier experiments^{1,2,7,31} and as can be seen the cross section for reaction (14a) rises from threshold to about $7 \mu\text{b}$ around 2 GeV and then drops rapidly to about $2 \mu\text{b}$ at 7.5 GeV.

From SU(3) it is expected that the $\omega\pi\gamma$ coupling is much larger³² than the $\rho\pi\gamma$ coupling,

$$\Gamma(\omega\pi\gamma) : \Gamma(\rho\pi\gamma) = 9 : 1. \quad (15)$$

Thus one-pion exchange (OPE) can contribute more to reaction (14a) than to reaction (6). We therefore attempted to fit the data of Fig. 16(a) (for $E_\gamma \geq 2.0 \text{ GeV}$) to a curve of the type

$$\sigma(\gamma p \rightarrow \omega p) = C_{\text{OPE}} E_\gamma^{-\alpha_1} + C_{\text{diff}} E_\gamma^{-\alpha_2}, \quad (16)$$

where E_γ is the photon laboratory energy in GeV. The data is too meager for a detailed analysis. α_1 is expected to be²⁶ 1.6–2.5, like in other OPE-dominated reactions (see Sec. V C above) and α_2 should be small [perhaps $\approx 0.2 \pm 0.15$, like in our energy dependence of $\sigma(\rho^0)$, see Fig. 11(d)]. A fit of the data of Fig. 16(a) to Eq. (16), for fixed $\alpha_1 = 2.0$, $\alpha_2 = 0.0$, yields $C_{\text{OPE}} = 31 \pm 5$ and $C_{\text{diff}} = 1.5 \pm 0.3$, and describes nicely the data [see curves in Fig. 16(a)]. With these parameters we also obtain good agreement with experiment for both the production cross sections and ω -decay distributions.²⁹ The OPE part of the cross section is obtained by using a sharp-cutoff absorption model³³ and for the diffractive part we use $d\sigma/dt = A e^{Bt}$ with $B = 7.1 \pm 0.4 \text{ GeV}^{-2}$ as obtained in the last section for the ρ^0 [Fig. 11(c)]. Since the asymptotic ω cross section for the diffractive part is $\sigma_D = 1.5 \pm 0.3 \mu\text{b}$, we obtain

$$A(\omega) = \left. \frac{d\sigma}{dt}(\gamma p \rightarrow \omega p) \right|_{t=0}^{\text{diff}} = \sigma_D B = 11 \pm 2 \mu\text{b}/\text{GeV}^2. \quad (17)$$

This value, together with the corresponding forward ρ^0 cross section, will be used (see Sec. VII) for deriving the direct VDM³⁴ couplings of photons and vector mesons and for comparisons of our cross sections with Compton-scattering results.

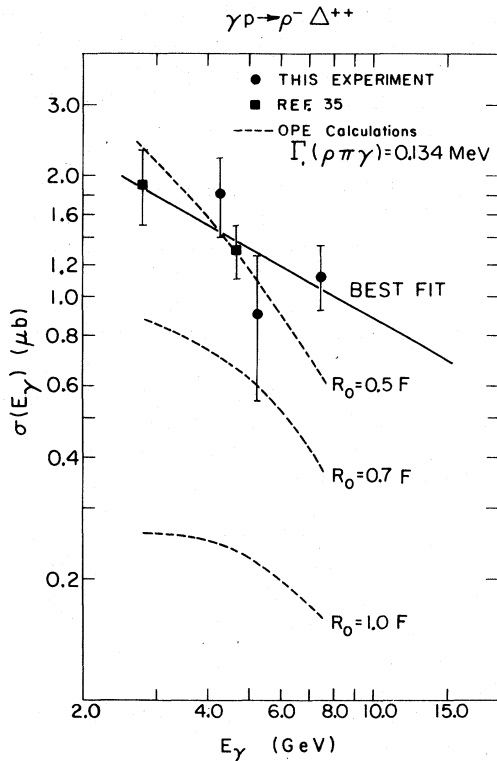


FIG. 17. $\gamma p \rightarrow \rho^- \Delta^{++}$ cross sections determined in this experiment and from Ref. 35, versus the photon energy E_γ . The full line is the best fit of the data to Eq. (18) which yields $a = 0.6 \pm 0.2$. The dashed curves are the OPE-calculated cross section for various absorption radii and fixed coupling [$\Gamma(\rho\pi\gamma) = 0.135$ MeV].

Ideally one would want to try to detect in relation (16) terms proportional to E_γ^{-1} and $E_\gamma^{-0.5}$, to account for possible A_2 and f^0 exchanges and their interference with the diffractive (Pomeranchukon) amplitude. Since our numbers of events are not sufficient to do this, we assume such terms are small.

C. $\rho^- \Delta^{++}$ Production

This reaction was also the subject of a separate publication³⁰ and will be discussed here very briefly. At the high energies (7.5 GeV) the associated $\rho^- \Delta^{++}$ production in reaction (14b) is well separated from the background and thus we have no difficulties in determining the cross sections in spite of their smallness. Our measured cross sections at all three energies are shown in Fig. 17 together with some recent measurements in the polarized-photon experiments³⁵ at 2.8 and 4.7 GeV.

In several early photoproduction experiments^{1,2} attempts were made to utilize reaction (14b) in order to estimate the $\rho\pi\gamma$ width, $\Gamma(\rho\pi\gamma)$. This was done by assuming the reaction mechanism to be

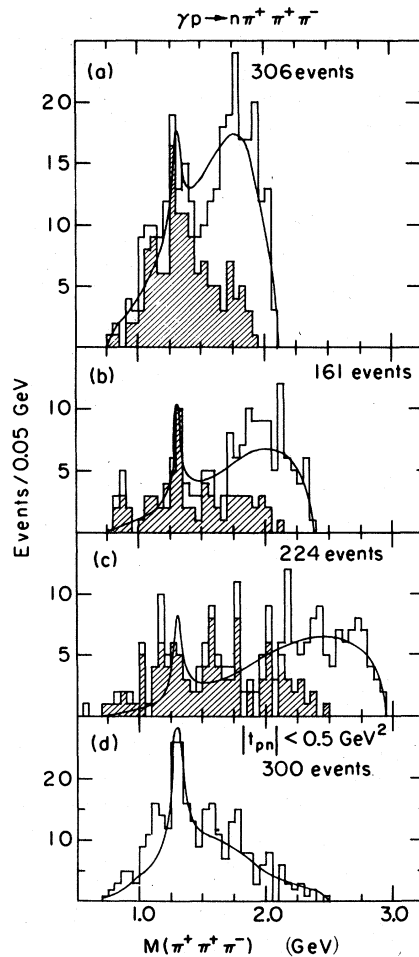


FIG. 18. $M(\pi^+ \pi^+ \pi^-)$ distribution in the reaction $\gamma p \rightarrow n \pi^+ \pi^+ \pi^-$ at (a) 4.3 GeV, (b) 5.25 GeV and (c) 7.5 GeV. The shaded areas represent events with $|t(p, n)| \leq 0.5$ GeV². (d) Mass distribution combining the three energies for above t cut. The curves are best fits to A_2 resonance [$M(A_2) = 1.30$ GeV, $\Gamma(A_2) = 0.1$ GeV] and phase space (see Table VIII).

one-pion exchange (OPE). More recently, in a γd experiment³⁶ at 4.3 GeV the reaction $\gamma n \rightarrow \omega \Delta^0$ was looked for and its cross section was found to be smaller than $0.5 \mu\text{b}$. It has been pointed out that this is in contradiction³⁶ to the assumption that reaction (14b) proceeds via OPE if the SU(3) relation (15) is correct. If relation (15) is even roughly accurate, the observed³⁶ upper limit on the ratio $\omega \Delta^0 / \rho^- \Delta^{++}$ would rule out OPE as the sole mechanism for reaction (14b).

The study of the energy dependence of reaction (14b) would serve as a test for the nature of the reaction mechanism. A best fit of the cross section (Fig. 17) to a power of the energy,

$$\sigma(\gamma p \rightarrow \rho^- \Delta^{++}) = C E_\gamma^{-a}, \quad (18)$$

TABLE VIII. Cross sections (in μb) obtained for the reactions $\gamma p \rightarrow p \pi^+ \pi^- \pi^0$ and $\gamma p \rightarrow n \pi^+ \pi^+ \pi^-$, and for resonance production therein. Associated resonance production is excluded from the single-resonance values and no correction (except ω) was made for decays into other channels.

Final state	E_γ (GeV)		
	3.7-4.7	4.7-5.8	6.8-8.2
$p \pi^+ \pi^- \pi^0$	18.2 ± 2.0	13.5 ± 1.5	11.8 ± 1.2
ωp^a	2.9 ± 0.4	2.3 ± 0.4	2.0 ± 0.3
$\rho^- \Delta^{++}$	1.8 ± 0.4	0.9 ± 0.35	1.1 ± 0.2
$\rho^0 \Delta^+$	0.1 ± 0.2	0.5 ± 0.2	0.3 ± 0.2
$\rho^+ \Delta^0$	0.1 ± 0.2	0.4 ± 0.3	0.2 ± 0.2
$\rho^- p \pi^+$	0.8 ± 0.5	1.7 ± 0.5	0.7 ± 0.4
$\rho^0 p \pi^0$	0.5 ± 0.5	b	0.9 ± 0.4
$\rho^+ p \pi^-$	1.8 ± 0.5	1.9 ± 0.5	1.1 ± 0.4
$\Delta^{++} \pi^0 \pi^-$	0.5 ± 0.4	0.6 ± 0.3	0.0 ± 0.1
$\Delta^+ \pi^+ \pi^-$	0.3 ± 0.3	0.0 ± 0.3	0.5 ± 0.2
$\Delta^0 \pi^+ \pi^0$	0.0 ± 0.3	0.0 ± 0.3	0.0 ± 0.5
$n \pi^+ \pi^+ \pi^-$	7.5 ± 1.5	4.6 ± 1.4	4.0 ± 1.2
$\Delta^- \pi^+ \pi^+$	1.4 ± 0.4	0.5 ± 0.3	0.2 ± 0.2
$n A_2^+$	0.8 ± 0.3	0.6 ± 0.3	0.3 ± 0.3
$\rho^0 n \pi^+$	1.2 ± 0.7	b	2.0 ± 0.6

^a Including 10% neutrals.

^b Unacceptable fits; see text.

gave $C = 3.5 \pm 1.2$ and $a = 0.6 \pm 0.2$, where σ is expressed in microbarns and E_γ in GeV. This fit indicates that very probably the reaction is *not* due to pure OPE, because of the following arguments³⁰: (a) In general, reactions believed dominated by OPE have an exponent²⁶ of about 2 (values of a between 1.6-2.5 are quoted in various compilations). (b) If we attempt to fit the data to a specific OPE model, the absorption model with sharp cutoff,³³ we find that for reasonable values of the absorption parameters (R between 0.8 and 1.0 F, which fits the shape of our differential cross sections) $\Gamma(\rho\pi\gamma)$ turns out to be about 0.5 MeV for $R = 0.8$ F and 0.85 MeV for $R = 1$ F. This width is about 4-6 times larger than the expected³⁷ $\rho\pi\gamma$ width [by Eq. (15), $\Gamma(\rho\pi\gamma) = \frac{1}{9}\Gamma(\omega\pi\gamma) = 0.134$ MeV] contradicting SU(3) and also unlikely on experimental grounds.³⁷

Thus we would tend to conclude that OPE does not dominate reaction (14b). More accurate data with polarized photons on both the production and decay of the resonances $\rho^- \Delta^{++}$ would be required for a definite determination of the mechanism of reaction (14). Quite possibly vector-meson exchanges are important in this reaction since (with in VDM) they would involve $\rho^0 \rho^+ \rho^-$ couplings which could be very strong.³⁸

D. The Reaction $\gamma p \rightarrow n A_2^+$

This reaction is the only clear quasi-two-body reaction in the n_{++} channel (13b). In Fig. 18 we

show the invariant-mass distributions $M(\pi^+ \pi^+ \pi^-)$ for the pions produced in reaction (13b), for a sample of clean monochromatic events [$P(\chi^2) \geq 0.05$ and $MM^2 = 0.6-1.2$ GeV² cuts were used]. Best fits to the mass distributions using 3- out of 4-body phase space and a single resonance (s-wave form) at all energies yielded the results shown in Fig. 18 and summarized in Table VIII. The fit to the 7.5-GeV data is rather poor and may indicate a more complicated structure in the A region. The A_2^+ production cross section seems to be decreasing with increase of E_γ as might be expected for an OPE-dominated reaction.

Our A_2^+ signal is associated mainly with ρ^0 decay and indeed we see no signal in events without associated ρ^0 , in agreement with the accepted branching ratio.³⁷ The shaded histograms in Fig. 18 for $|t(p, n)| < 0.5$ GeV² demonstrate that the A_2^+ production is associated with small momentum transfers. Best fits to the combined data of Fig. 18(d) yield a mass $m_A = 1.30 \pm 0.01$ GeV and width $\Gamma(A_2^+) = 0.13 \pm 0.046$ GeV, in agreement with other experiments.

In the notation of our previous work³⁹ and assuming that A_2^+ production in reaction (14c) is due to an OPE process, we get

$$\frac{d\sigma}{dt}(\gamma p \rightarrow n A_2^+) = \frac{\pi}{64} \frac{g_{\pi NN}^2}{4\pi} \frac{g_{A_2 \pi \gamma}^2}{4\pi} \frac{|t|(t-m_A^2)^4}{m_A^6 k^2 s(t-\mu^2)^2}, \quad (19a)$$

where $g_{\pi NN}^2/4\pi = 14.6$, k and s are photon momentum and total energy squared in the over-all c.m. system and μ is the pion mass. Introducing final-state absorption corrections³³ into Eq. (19a) we may derive from our experiment the $A_2 \pi \gamma$ coupling constant $g_{A_2 \pi \gamma}$ (we used twice the cross sections of Table VIII to account for $\rho^+ \pi^0$ decays). From it we obtain the partial decay width,

$$\Gamma(A_2^+ \rightarrow \gamma \pi^+) = \frac{1}{10} \frac{g_{A_2 \pi \gamma}^2}{4\pi} \frac{q^5}{m_A^4}, \quad (19b)$$

where q is the photon momentum in $A_2 - \pi \gamma$ decay.

Again the problem of choosing the absorption radius arises. We find for $R = 1.0$ F (the hadronic reaction value) that $\Gamma(A_2 \pi \gamma) = 0.6$ MeV while for $R = 0.8$ F (used for our ω -photoproduction results) $\Gamma(A_2 \pi \gamma) = 0.3$ MeV. Hence we conclude that within a factor of 2,

$$\Gamma(A_2 \pi \gamma) \approx 0.5 \text{ MeV}.$$

If we assume VDM to hold in the A_2 rest frame we may write³⁹

$$g_{A_2 \pi \gamma}^2 = \frac{\alpha}{4} \left(\frac{\gamma \rho^2}{4\pi} \right)^{-1} g_{A_2 \rho \pi}^2. \quad (20)$$

With the effective value $\gamma_0^2/4\pi = 0.32$ that is derived

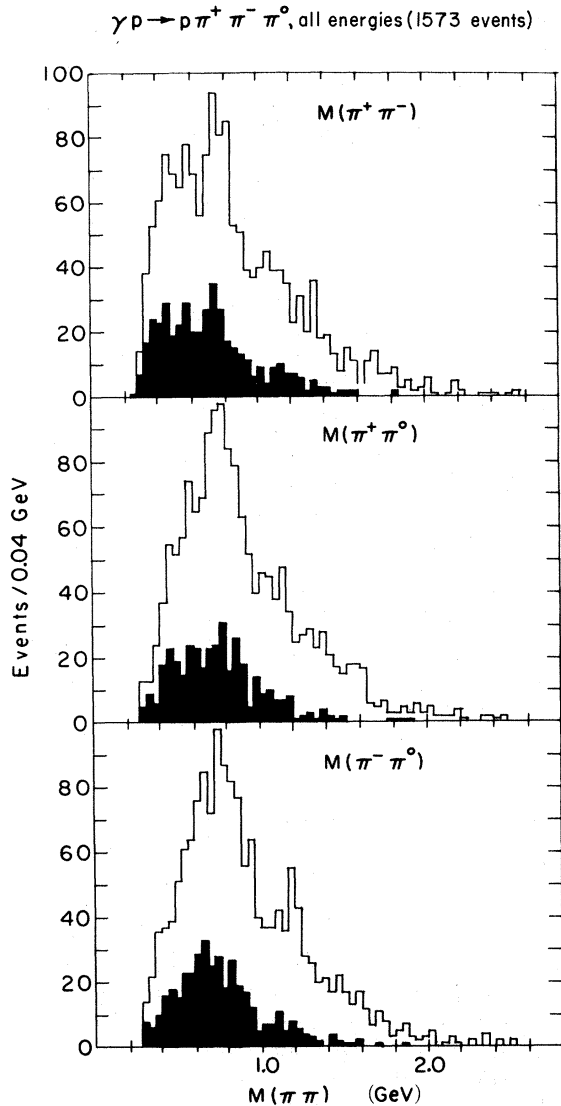


FIG. 19. $M(\pi\pi)$ distribution for the reaction $\gamma p \rightarrow \rho \pi^+ \pi^- \pi^0$ at 4.3, 5.25, and 7.5 GeV combined. Solid areas represent events with $|t(\gamma, \pi\pi)| \leq 0.5 \text{ GeV}^2$. All ω^0 [$M(\pi^+ \pi^- \pi^0) < 0.81 \text{ GeV}$] and $\rho^- \Delta^{++}$ events [$M(\pi^- \pi^0) = 0.60-0.85 \text{ GeV}$ and $M(p \pi^+) = 1.15-1.30 \text{ GeV}$] are removed.

in Sec. VII, we obtain for the VDM prediction $\Gamma(A_2^+ \rightarrow \gamma \pi^+) \approx 2 \text{ MeV}$, while the storage-ring value gives $\approx 1.2 \text{ MeV}$. Considering the uncertainties in the data and in the treatment the disagreement should not be considered serious, but may indicate that VDM plus OPE is not sufficient to explain the data. Much more data would be required for a better examination of VDM in A_2 photoproduction.

E. Inelastic ρ Production

As was noted already in previous experiments^{2,4,5} there is substantial production of ρ 's in the inelas-

tic reaction

$$\gamma p \rightarrow \rho + N\pi. \quad (21)$$

The relative abundance of ρ^0 and ρ^\pm in reaction (21) depends on the production mechanism. ρ^\pm production is forbidden in a diffractive process while ρ^0 production will be suppressed if the ρ 's are produced via $I=1$ exchange to the dominant isovector part of the photon. Thus the cross sections for ρ production in various charge states and its t distribution may indicate the production mechanism.

The invariant-mass plots of the $\pi^+ \pi^0$, $\pi^+ \pi^-$, and $\pi^- \pi^0$ produced in the $p + 0$ final state is shown in Fig. 19, combining the three annihilation energies. Here ω and $\rho^- \Delta^{++}$ events have been removed. Darkened events are those with small momentum transfer to the dipion system. Photoproduction of ρ^+ , ρ^0 , and ρ^- is clearly visible but not all is peripheral. We performed a multidimensional fit to the data, assuming the production of ρ^+ , ρ^- , ρ^0 , Δ^{++} , Δ^+ , and Δ^0 both in associated and unassociated production, and a 4-body phase-space background. The results of the fits, at the three annihilation energies, are given in Table VIII. None of the cross sections changed significantly when a possible A_2^0 production term was introduced. For the 5.25-GeV data we were unable to obtain a good fit to the $\pi^+ \pi^-$ mass spectrum in either the $p + 0$ or n^{++} channels, because the ρ^0 signal was anomalously broad and the background unlike phase space. We are unable to account for this effect, which does not occur in the other mass combinations. Since the signal is clear at our other energies, we prefer not to give a cross section for unassociated ρ^0 in the 5.25-GeV data.

In order to gain information about the possible production mechanism of the mesons produced in channel (13) we plot in Fig. 20 the $\pi^+ \pi^-$ and $\pi^\pm \pi^0$ invariant masses for events with small momentum transfer ($|t| \leq 0.5 \text{ GeV}^2$) between the photon and the vector meson for the three annihilation energies combined. Excluded from the graphs are all events having ω , $\rho^- \Delta^{++}$, or $A_2^+(\pi^+ \pi^+ \pi^-)$ production. Thus reflections from the quasi-two-body reactions discussed above are eliminated as much as possible. We observe from Fig. 20 that there is significant ρ^0 production, associated with both $p\pi^0$ and $n\pi^+$, remaining after the above cuts and that this production is peripheral. The signal for charged ρ^\pm production at small $|t|$ values is much weaker. If we associate this peripherally produced ρ^0 with a "diffraction dissociation" process,⁴⁰ we would conclude that the ratio of elastic diffractive ρ^0 photoproduction to inelastic diffractive production is about 30 (i.e., $15 \mu\text{b}/0.5 \mu\text{b}$). This is similar to the ratios obtained in pion-nucleon and nucleon-nucleon reac-

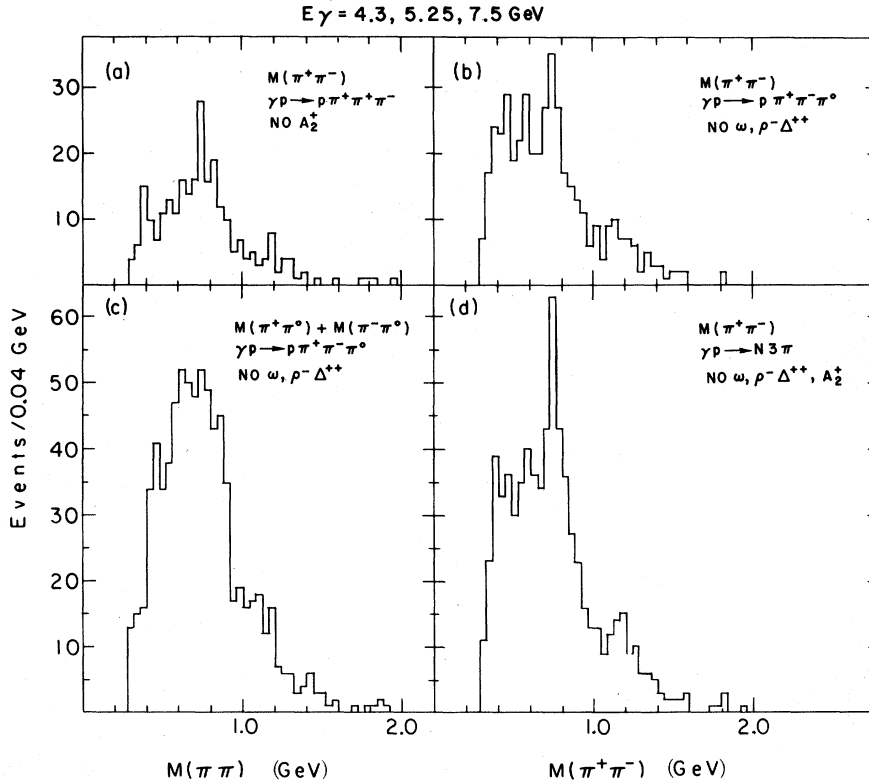


FIG. 20. Peripheral $M(\pi\pi)$ distribution [$|t(\gamma, \pi\pi)| \leq 0.5 \text{ GeV}^2$] for reaction (13) at all energies. (a) $M(\pi^+\pi^-)$ for reaction (13b), A_2^+ events [$M(\pi^+\pi^+\pi^-) = 1.25-1.35 \text{ GeV}$] removed. (b) $M(\pi^+\pi^-)$ for reaction (13a), ω and $\rho^-\Delta^{++}$ events removed. (c) $M(\pi^+\pi^0)$ and $M(\pi^-\pi^0)$ for reaction (13a), ω and $\rho^-\Delta^{++}$ removed. (d) Sum of (a) and (b).

tions.⁴⁰ We wish to emphasize that our signal is small and thus we do not have enough statistics to study it in detail or even to prove that it is really diffractive. However, it is worth noting that when we plot the invariant masses of the $N\pi$ system associated with the ρ^0 (Fig. 21), we *do not* see evidence for the production of any of the known $N^*(I = \frac{1}{2})$ resonances. In fact, we note that the majority of the inelastic ρ^0 production is associated with small momentum transfer to the nucleon. Though this may indicate photon association into $\rho\pi$ systems, we see no significant 3π structures other than A_2^+ . It has been suggested that $\rho^0 N^*$ associated production may occur at much higher photon energies.⁴¹

Finally we wish to comment that the inelastic ρ production observed in this experiment, the final states $\rho^0\pi^-p$ and $\omega\pi^-p$ observed in γn reactions³⁶ and the reactions $\gamma p \rightarrow V^0\pi^-\Delta^{++}$ ($V^0 = \rho^0, \omega$) which were reported previously,^{4,5} need not all have the same production mechanism. Some may be diffractive (like the ρ^0 in Fig. 20 above and that observed in γn reactions³⁶), others may be due to OPE (ω production), and ρ^\pm production may be due to charged-vector-meson exchange since the $\rho^0\rho^+\rho^-$ coupling could be large.³⁸

F. Inelastic Nucleon Isobar Production

A summary of the cross sections for baryon-resonance production at all energies is also given in Table VIII. These cross sections are rather small and we do not notice any quasi-two-body reaction other than $\rho^-\Delta^{++}$ that was discussed already. Δ^- production in reaction (13b) is large at 4.3 GeV and decreases rapidly with energy. The $(N\pi)^+$ mass plot associated with ρ^0 production (Fig. 21) shows general enhancement at low masses but, as mentioned before, no N^* 's are resolved. Similarly, the $p\pi^-$ system associated with ρ^+ production does not show any resonance structure.

VII. VECTOR-DOMINANCE-MODEL TESTS AND THE PHOTON-VECTOR-MESON COUPLINGS

In the previous sections we have obtained the $\rho^0 p$ differential cross sections and have separated the ωp cross section into its energy-dependent part and constant (presumably diffractive) part. Assuming the slope for ρ^0 and ω production to be the same, the diffractive ρ^0/ω ratio of cross sections in the forward direction at our highest energy, 7.5 GeV, is just

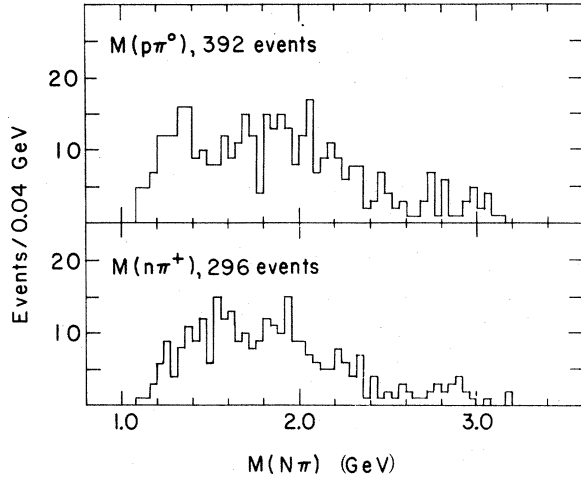


FIG. 21. $M(p\pi^0)$ and $M(n\pi^+)$ distribution in the reactions $\gamma p \rightarrow p\pi^+\pi^-\pi^0$ and $n\pi^+\pi^+\pi^-$, respectively, for the events with $M(\pi^+\pi^-) = 0.65-0.85$ GeV. ω , ρ - Δ^{++} , and A_2^+ events are removed from the sample. From our fits about half the events in this figure originate in the reaction $\gamma p \rightarrow \rho^0 N\pi$.

$$\frac{A(\rho^0 p)}{A(\omega p)} = \frac{\sigma(\rho p)}{\sigma(\omega p)} = \frac{14.3 + 1.3}{1.5 \pm 0.3} = 9.5 \pm 2.3. \quad (22)$$

This ratio, by SU(3) and VDM^{32,34} should be 9:1. In colliding-beam experiments, when the photon is on the vector-meson mass shell, the ratio (22) above was found⁴² to be 7.5 ± 1.5 , not in disagreement with our value.

Within the framework of VDM, the relation between the amplitude for Compton scattering and photoproduction of transverse vector mesons, V_t^0 , required for our comparisons, can be written as follows:

$$a(\gamma p \rightarrow \gamma p) = \sum_{V^0} \frac{\sqrt{\alpha\pi}}{\gamma_V} a(\gamma p \rightarrow V_t^0 p), \quad (23)$$

where $V^0 = \rho^0$, ω , ϕ , plus any other vector mesons coupled to the photon, and $\gamma_V^2/4\pi$ is the usual γV coupling constant. The optical theorem for the spin-averaged forward cross section can be written as

$$\frac{\sigma_T^2}{16\pi} = \frac{1}{1 + |\eta|^2} \frac{d\sigma}{dt} (t=0), \quad (24)$$

where $\eta = \text{Re}a(0)/\text{Im}a(0)$.

From (23) and (24) we then obtain

$$\sigma_T(\gamma p) = \left(\frac{\gamma_{\rho, \text{eff}}^2}{4\pi} \right)^{-1/2} \times \sum_{V^0} \left[\frac{4\pi\alpha}{1 + \eta_V^2} \left(\frac{\gamma_V}{\gamma_V} \right)^2 \frac{d\sigma}{dt} (\gamma p \rightarrow V_t^0 p)_{t=0}^{\text{diff}} \right]^{1/2}. \quad (25)$$

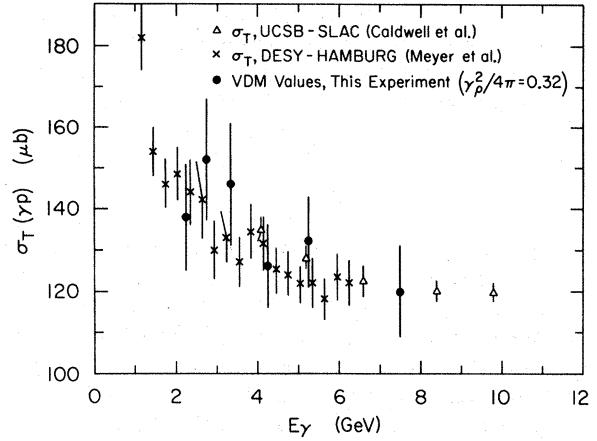


FIG. 22. Comparison of measured γp total cross sections of Ref. 43, with VDM predictions based upon present data, for $\gamma_{\rho}^2/4\pi = 0.32$ (see text).

Knowing the forward vector-meson cross section and using the recent⁴³ measurements of $\sigma_T(\gamma N)$, we are able to determine the effective value of $\gamma_{\rho}^2/4\pi$ in Eq. (25) ($|\eta|^2$ is estimated⁴⁴ to be small, about 0.04).

Our experimental values for the right-hand side of (25) are given in Fig. 22 (average of Söding and phenomenological cross sections, Table VI) with the effective $\gamma_{\rho}^2/4\pi$ adjusted for best agreement with the σ_T measurements⁴³ above 3.7 GeV. The magnitude of the ω and ϕ diffractive cross sections were taken from Sec. VI B and from Anderson *et al.*¹⁷ while the ratio of couplings were obtained from Eq. (22) above. For $\gamma_{\rho, \text{eff}}^2/4\pi = 0.32 \pm 0.03$ (and not 0.50 as obtained in the storage-ring experiments⁴²) the s dependence of both processes are similar. It should be noted that a similar comparison made on 4.3-GeV γd data³⁶ found an effective $\gamma_{\rho}^2/4\pi = 0.28 \pm 0.04$.

The recently reported direct measurements of Compton scattering cross sections²⁴ allow a further test of the VDM idea, which avoids the uncertainty of the extrapolation to $t=0$ for the ρ^0 data, and the assumption of a small real part in Compton scattering. If the amplitudes (23) for vector-meson production all have the same phase (e.g., all imaginary) and spin structure, we obtain at all t

$$\frac{d\sigma}{dt} (\gamma p \rightarrow \gamma p) = \frac{\alpha}{4} \left(\frac{\gamma_{\rho, \text{eff}}^2}{4\pi} \right)^{-1} \times \left[\sum_{V^0} \frac{\gamma_V}{\gamma_V} \left(\frac{d\sigma}{dt} (\gamma p \rightarrow V_t^0 p) \right)^{1/2} \right]^2. \quad (26)$$

In the more general case, VDM would require the

left-hand side of (26) to be \leq the right-hand side (from the density-matrix elements of Fig. 12 we conclude that all the ρ^0 is transverse). In Fig. 23 we present our results for the right-hand side of Eq. (26) for the above value of $\gamma_\rho^2/4\pi$. We use our standard values (Table VII) for the ρ^0 part, and make the comparison for $E_\gamma > 4$ GeV, where the incoherent background is small. For the ω and ϕ contributions we used, respectively, our measured ω cross sections and the ϕ data of Ref. 17. In Fig. 23 we also show the directly measured Compton scattering cross sections²⁴ in hydrogen. Note that our points are *raw data* obtained from the number of dipion pairs with mass in the interval 0.715–0.815 GeV. In this mass interval the Söding interference term is expected to roughly cancel and other backgrounds are small (see Sec. V). The lines in Fig. 23 correspond to the ρ^0 standard slopes (Table VI) and are normalized in the forward direction to the sum of the ρ^0 standard cross section plus the ω and ϕ diffractive forward cross sections as in (25). Thus the curves represent our best estimate for the right-hand side of (26) assuming only diffractive contributions. Excellent agreement between our photoproduction data and Compton scattering via the VDM Eq. (26) is obtained at all s and t values where data on both reactions are available.

Because the forward cross section was used already in (25) to determine the couplings, the real meaning of the agreement observed in Fig. 23 is that the slope that we observe in photoproduction (average of 7.1 ± 0.4 GeV⁻²; see Table VI) is in agreement with Compton scattering. This is a somewhat different conclusion than that reached in Ref. 24, since the slope they assumed for ρ^0 photoproduction was about 8.5 GeV⁻².

In this context we must note (see Sec. V B) that our forward ρ cross sections and slopes are lower than some counter experiment values.¹² This discrepancy could be accounted for by the “inelastic” ρ production observed in this and other experiments,⁴⁵ by using a different mass interval to define the ρ^0 or a different extrapolation function.

We conclude from our comparison of photoproduction and Compton scattering that the two processes have the same t dependence, and within large errors and over a restricted range of comparison the same s dependence, so that with the variation of only one parameter we can satisfy the VDM tests. The effective *magnitude* of $\gamma_\rho^2/4\pi$ that we require is roughly comparable to, but still smaller than, the storage-ring⁴² value (with photons on the vector-meson mass shell). It is worth noting that in comparison of single- π photoproduction with vector-meson production in pion experiments⁴⁶ one also usually obtains rough agreement in mag-

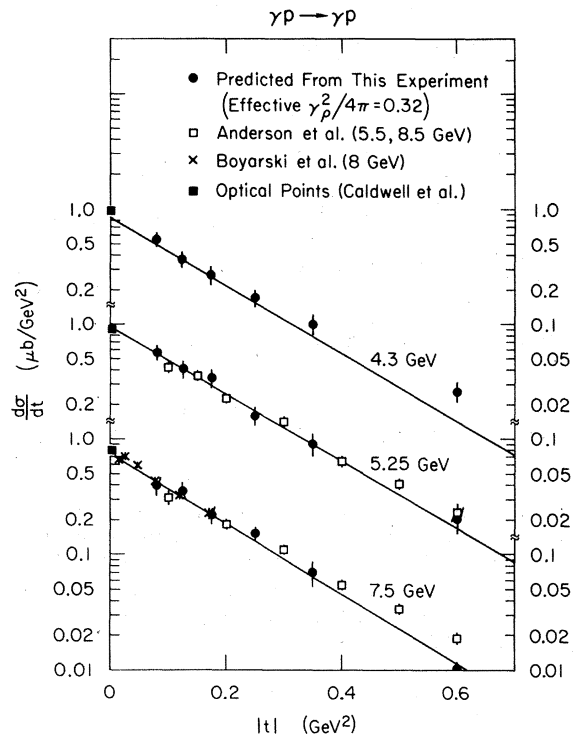


FIG. 23. $d\sigma/dt$ for Compton scattering calculated from the present photoproduction data of Table VII using Eq. (26) and $\gamma_\rho^2/4\pi = 0.32$. The straight lines represent our standard fits (see text). The VDM-predicted cross sections are compared with recent Compton-scattering measurements of Ref. 24 at 5.5, 8, and 8.5 GeV.

nitude with the VDM predictions for coupling constants around 0.30, but in this case there may be disagreement in the t dependence of the two processes.⁴⁷

Thus VDM appears to be violated in its most restrictive form. The meaning of the effective value for $\gamma_\rho^2/4\pi$ found in photoproduction on hydrogen is not at all clear. From ρ photoproduction on complex nuclei¹² and deuterium,⁴⁸ values of $\gamma_\rho^2/4\pi \sim 0.7$ are found, so that simply a change of coupling with meson mass cannot account for the deviation from the storage-ring value. It is conceivable that more vector mesons (or several pion structures having the quantum numbers of the photon) are required to saturate relation (25), or that the V -nucleon scattering amplitude changes when the V is off the mass shell.⁴⁹ Similar conclusions were noted in Ref. 36, in a study of γd reactions. (See also Sec. V D.)

ACKNOWLEDGMENTS

We gratefully acknowledge the help of many people. Some of the present authors also worked on the polarized-photon experiment of the SLAC-

Berkeley-Tufts collaboration, so that many of the techniques described were developed for both investigations, and such borrowings are noted in the text. In particular, we thank G. Wolf (working on this experiment initially), I. O. Skillicorn, K. Mofeit, H. Spitzer, and others of the SBT collaboration, who generously shared their ideas and programs. We thank D. Yennie, H. Harari, and

F. Gilman for useful discussion, and Z. Guiragosian, P. Klein, E. Pickup, T. Tan, E. Peleg, G. Vishinski and E. Kogan for help in the initial phases. In addition, we are grateful to A. Kilert, the SLAC bubble-chamber operations crew and the SLAC Experimental Facilities Group for the successful runs and Mrs. M. Tartar, K. Eymann, and our scanning personnel for their diligence.

*Work supported in part by the U. S. Atomic Energy Commission.

†On leave from Max Planck Institute, Munich, West Germany.

¹Cambridge Bubble Chamber Group, Phys. Rev. 146, 994 (1966); 155, 1468 (1967); 169, 1080 (1968).

²Aachen-Berlin-Bonn-Hamburg-Heidelberg-München Collaboration, Phys. Rev. 175, 1669 (1968); 188, 2060 (1969).

³M. Davier *et al.*, Phys. Rev. D 1, 790 (1970).

⁴J. Ballam *et al.*, Phys. Rev. Letters 21, 1541 (1968); 21, 1544 (1968); Phys. Letters 30B, 421 (1969).

⁵Y. Eisenberg *et al.*, Phys. Rev. Letters 22, 669 (1969).

⁶H. H. Bingham *et al.*, Phys. Rev. Letters 24, 955 (1970); J. Ballam *et al.*, *ibid.* 24, 960 (1970); 24, 1467(E) (1970); also, Phys. Rev. D (to be published).

⁷J. Ballam *et al.*, Phys. Rev. Letters 24, 1364 (1970); 26, 155(E) (1970).

⁸H. H. Bingham *et al.*, Phys. Rev. Letters 25, 1223 (1970).

⁹J. Ballam *et al.*, Nucl. Instr. Methods 73, 53 (1969).

¹⁰Y. S. Tsai, Phys. Rev. 137, B730 (1965).

¹¹T. M. Knasel, DESY Report No. DESY 70/3, 1970 (unpublished).

¹²G. McClellan *et al.*, Phys. Rev. Letters 22, 374 (1969); H. Blechschmidt *et al.*, Nuovo Cimento 52A, 1348 (1967); H. Alvensleben *et al.*, Phys. Rev. Letters 23, 1058 (1969); W. G. Jones *et al.*, *ibid.* 21, 586 (1969); M. Davier *et al.*, *ibid.* 21, 841 (1968), and Phys. Letters 28B, 619 (1969); R. Anderson *et al.*, Phys. Rev. D 1, 27 (1970).

¹³E. Burns and D. Drijard, Technical Note No. 143, Trilling-Goldhaber Group, Lawrence Radiation Laboratory, 1968 (unpublished).

¹⁴L. Criegee *et al.*, Phys. Letters 28B, 282 (1968); G. Diambri-Palazzi *et al.*, Phys. Rev. Letters 25, 478 (1970).

¹⁵It has been suggested that helicity conservation is an asymptotic property of diffraction scattering; see F. J. Gilman *et al.*, Phys. Letters 31B, 387 (1970).

¹⁶A. M. Boyarski *et al.*, Phys. Rev. Letters 22, 148 (1969); 25, 695 (1970).

¹⁷G. McClellan *et al.*, Phys. Rev. Letters 23, 718 (1969); N. Hicks *et al.*, Phys. Letters 29B, 602 (1969); R. Anderson *et al.*, Phys. Rev. D 1, 27 (1970); F. Bulos *et al.*, Phys. Rev. Letters 26, 149 (1971); H. Alvensleben *et al.*, *ibid.* 26, 273 (1971).

¹⁸There is no consensus about what an "unskewed" ρ^0 should look like, so we compare here with the s -wave nonrelativistic form using $m_\rho = 765$ MeV, $\Gamma_\rho = 140$ MeV, arguing that it gives a minimum expected intensity. See, e.g., H. Harari and Y. Zarmi, Phys. Rev. 187, 2230

(1969).

¹⁹P. Söding, Phys. Rev. Letters 19, 702 (1965); A. S. Krass, Phys. Rev. 159, 1496 (1967).

²⁰M. Ross and L. Stodolsky, Phys. Rev. 149, 1172 (1966); G. Kramer and J. L. Uretsky, *ibid.* 181, 1918 (1969); P. D. Mannheim and U. Maor, Phys. Rev. D 2, 2105 (1970).

²¹S. Drell, Phys. Rev. Letters 5, 278 (1960).

²²E. Ferrari and F. Selleri, Phys. Rev. Letters 7, 387 (1969). The use of such a form factor improves the fits, but may be questionable in photoproduction. (D. R. Yennie, private communication.)

²³J. Pumplin, Phys. Rev. D 2, 1859 (1970); T. Bauer, Phys. Rev. Letters 25, 485 (1970). We thank D. R. Yennie for discussion on this and the "standard" method.

²⁴R. L. Anderson *et al.*, Phys. Rev. Letters 25, 1218 (1970); A. M. Boyarski *et al.*, *ibid.* 26, 1600 (1971).

²⁵With all momenta transformed to the rest system of the $\pi^+\pi^-$, the helicity-system z axis is taken opposite the recoil proton direction, the y axis in the direction of $\vec{p}_{\text{recoil}} \times \vec{k}$, where \vec{k} is the photon momentum and $\hat{x} = \hat{y} \times \hat{z}$, and the π^+ direction is the polarization analyzer.

²⁶D. R. O. Morrison, Phys. Letters 22, 528 (1966); A. Shapira *et al.*, Nucl. Phys. B 23, 583 (1970); Z. M. Ma *et al.*, Phys. Rev. Letters 24, 1031 (1970).

²⁷With all momenta transferred to the $p\pi^+$ rest system, the Jackson-system z axis is taken along the direction of the incoming proton, the y axis in the direction of $\vec{\pi}^- \times \vec{p}_{\text{in}}$, where $\vec{\pi}^-$ is the direction of the π^- , $\hat{x} = \hat{y} \times \hat{z}$, and the outgoing proton is the spin analyzer.

²⁸G. Veneziano, Nuovo Cimento 57A, 190 (1968); J. G. Cordes and P. J. O'Donnell, Phys. Rev. Letters 20, 146 (1968); J. A. Shapiro, Phys. Rev. 179, 1345 (1969).

²⁹Y. Eisenberg *et al.*, Phys. Letters 34B, 439 (1971).

³⁰J. Ballam *et al.*, Phys. Rev. Letters 26, 995 (1971).

³¹M. Davier *et al.*, Phys. Letters 28B, 619 (1969).

³²See, for example, H. Harari, Phys. Rev. 155, 1565 (1967).

³³B. Haber and G. Yekutieli, Phys. Rev. 160, 1410 (1967).

³⁴J. J. Sakurai, Ann. Phys. (N.Y.) 11, 1 (1960); M. Gell-Mann and F. Zachariasen, Phys. Rev. 124, 953 (1961).

³⁵J. Ballam *et al.*, paper submitted to the Fifteenth International Conference on High Energy Physics, Kiev, U.S.S.R., 1970 (unpublished), and private communication.

³⁶Y. Eisenberg *et al.*, Phys. Rev. Letters 25, 764 (1970); Nucl. Phys. B 25, 499 (1971); Weizmann Institute Report No. WIS 71/9, 1971 (unpublished).

³⁷Particle Data Group, Phys. Letters 33B, 1 (1970). Upper limit on the $\rho\pi\gamma$ width is given by G. Fidecaro *et al.*, Phys. Letters 23, 163 (1966).

³⁸S. M. Berman and U. Maor, *Nuovo Cimento* 36, 483 (1965); R. B. Clark, *Phys. Rev.* 187, 1993 (1969); *Phys. Rev. D* 1, 2152 (1970); M. Glück and S. Wagner, *ibid.* 3, 1669 (1971).

³⁹Y. Eisenberg *et al.*, *Phys. Rev. Letters* 23, 1322 (1969). For the $A_2\pi\gamma$ matrix element, see H. Høgaasen *et al.*, *Nuovo Cimento* 42A, 323 (1966).

⁴⁰M. L. Good and W. D. Walker, *Phys. Rev.* 120, 1854 (1960). See also D. R. O. Morrison, rapporteur's talk in *Proceedings of the Fifteenth International Conference on High Energy Physics, Kiev, U.S.S.R., 1970* (Atomizdat, Moscow, 1971), and CERN Report No. CERN/PHYS 70-64 (unpublished).

⁴¹G. Wolf, *Nucl. Phys.* B26, 317 (1971).

⁴²J. E. Augustin *et al.*, *Phys. Letters* 28B, 508 (1969); 28B, 513 (1969); 28B, 517 (1969).

⁴³D. O. Caldwell *et al.*, *Phys. Rev. Letters* 25, 609 (1970); 25, 613 (1970); H. Meyer *et al.*, *Phys. Letters* 33B, 189 (1970).

⁴⁴M. Damashek and F. J. Gilman, *Phys. Rev. D* 1, 1319 (1970).

⁴⁵See analysis of G. Wolf, DESY Report No. 70/64 (unpublished).

⁴⁶R. Diebold and J. A. Poirier, *Phys. Rev. Letters* 20, 1532 (1968); 22, 906 (1969); Z. Guiragossian and A. Levy, *Phys. Letters* B30, 48 (1969). A recent comparison is given by D. Schildknecht, DESY Report No. 70/31 (unpublished).

⁴⁷F. Bulos *et al.*, *Phys. Rev. Letters* 26, 1457 (1971).

⁴⁸R. L. Anderson *et al.*, *Phys. Rev. D* 4, 3245 (1971).

⁴⁹A. Schwimmer and D. R. Yennie (private communication).